



# Distributed Fiber-Optic Hydrogeophysics

Scott W. Tyler, John S. Selker, Thom Bogaard,  
Nick van de Giesen, Juan Aguilar-López

# *Distributed Fiber-Optic Hydrogeophysics*

*The Groundwater Project*

i

***Scott W. Tyler***

*Professor*

*Department of Geological Sciences and Engineering  
University of Nevada  
Reno, Nevada, USA*

***John S. Selker***

*Professor*

*Department of Biological and Ecological  
Engineering  
Oregon State University  
Corvallis, Oregon, USA*

***Thom Bogaard***

*Professor*

*Water Management Department  
Delft University of Technology  
Delft, The Netherlands*

***Nick van de Giesen***

*Professor*

*Water Management Department  
Delft University of Technology  
Delft, The Netherlands*

***Juan Aguilar-López***

*Assistant Professor,*

*Hydraulic Engineering Department  
Delft University of Technology  
Delft, The Netherlands*

***Distributed Fiber-Optic  
Hydrogeophysics***

*The Groundwater Project  
Guelph, Ontario, Canada  
Version 4, March 2023*

All rights reserved. This publication is protected by copyright. No part of this book may be reproduced in any form or by any means without permission in writing from the authors (to request permission contact: [permissions@gw-project.org](mailto:permissions@gw-project.org)). Commercial distribution and reproduction are strictly prohibited.

The Groundwater Project (The GW-Project) works can be downloaded for free from [gw-project.org](http://gw-project.org). Anyone may use and share [gw-project.org](http://gw-project.org) links to download GW-Project's work. It is not permissible to make GW-Project documents available on other websites nor to send copies of the documents directly to others. Kindly honor this source of free knowledge that benefits you and all those who want to learn about groundwater.

Copyright © 2022 Scott W. Tyler, John S. Selker, Nick van de Giesen, Thom Bogaard, and Juan Aguilar-López (The Authors)

Published by the Groundwater Project, Guelph, Ontario, Canada, 2022.

Tyler, Scott W.

Distributed Fiber-Optic Hydrogeophysics / Scott W. Tyler, John S. Selker, Nick van de Giesen, Thom Bogaard, and Juan Aguilar-López - Guelph, Ontario, Canada, 2022.

49 pages

ISBN: 978-1-77470-031-0

DOI: <https://doi.org/10.21083/978-1-77470-031-0>

Please consider signing up for the GW-Project mailing list to stay informed about new book releases, events, and ways to participate in the GW-Project. When you sign up for our email list it helps us build a global groundwater community. [Sign up](#).

APA (7<sup>th</sup> ed.) Citation: Tyler, S.W., Selker, J.S., Van de Giesen, N., Bogaard, T., & Aguilar-López, J. (2022). *Distributed fiber-optic hydrogeophysics*. The Groundwater Project. [doi.org/10.21083/978-1-77470-031-0](https://doi.org/10.21083/978-1-77470-031-0).



*Domain Editors:* Eileen Poeter and John Cherry

*Board:* John Cherry, Paul Hsieh, Ineke Kalwij, Stephen Moran, Everton de Oliveira and Eileen Poeter

*Steering Committee:* John Cherry, Allan Freeze, Paul Hsieh, Ineke Kalwij, Douglas Mackay, Stephen Moran, Everton de Oliveira, Beth Parker, Eileen Poeter, Ying Fan, Warren Wood, and Yan Zheng.

*Cover Image:* Troy Gilmore

## Dedication

The authors dedicate this work to all of those who have gone before us in the study of hydrology, hydrogeology and soil physics. It is upon their shoulders that we were able to stand.

# Table of Contents

<b>DEDICATION</b> .....	<b>III</b>
<b>TABLE OF CONTENTS</b> .....	<b>IV</b>
<b>THE GROUNDWATER PROJECT FOREWORD</b> .....	<b>V</b>
<b>FOREWORD</b> .....	<b>VI</b>
<b>PREFACE</b> .....	<b>VII</b>
<b>ACKNOWLEDGMENTS</b> .....	<b>VIII</b>
<b>1 INTRODUCTION</b> .....	<b>1</b>
<b>2 BASIC PRINCIPLES OF FIBER SENSING</b> .....	<b>2</b>
<b>3 FIBER-OPTIC DISTRIBUTED TEMPERATURE SENSING (DTS)</b> .....	<b>5</b>
3.1 DTS APPLICATIONS IN HYDROGEOLOGY.....	11
<b>4 STRAIN MEASUREMENT</b> .....	<b>20</b>
4.1 BRILLOUIN DISTRIBUTED STRAIN SENSING (BDSS) .....	20
4.2 STRAIN AND STRAIN RATE MEASUREMENT: DISTRIBUTED ACOUSTIC SENSING (DAS).....	21
<b>5 CONCLUSION: THE FUTURE LOOKS OPTICALLY BRIGHT!</b> .....	<b>26</b>
<b>6 EXERCISES</b> .....	<b>27</b>
EXERCISE 1.....	27
EXERCISE 2.....	28
EXERCISE 3.....	29
<b>7 REFERENCES</b> .....	<b>30</b>
<b>8 EXERCISE SOLUTIONS</b> .....	<b>38</b>
SOLUTION EXERCISE 1 .....	38
SOLUTION EXERCISE 2 .....	40
SOLUTION EXERCISE 3 .....	44
<b>9 NOTATIONS</b> .....	<b>45</b>
<b>10 ABOUT THE AUTHORS</b> .....	<b>46</b>
<b>MODIFICATIONS TO ORIGINAL RELEASE</b> .....	<b>A</b>

## The Groundwater Project Foreword

The Year 2022 marks an important year for groundwater because the United Nations Water Members and Partners have chosen the theme of this year's March 22 World Water Day to be: "Groundwater: making the invisible visible". The goal of the Groundwater Project (GW-Project) is in sync with this theme.

The GW-Project, a registered charity in Canada, is committed to contributing to advancement in groundwater education and brings a unique approach to the creation and dissemination of knowledge for understanding and problem-solving. The GW-Project operates the website <https://gw-project.org/> as a global platform for the democratization of groundwater knowledge, founded on the principle that:

*"Knowledge should be free and the best knowledge should be free knowledge." Anonymous*

The mission of the GW-Project is to promote groundwater learning. This is accomplished by providing accessible, engaging, high-quality, educational materials, free-of-charge online in many languages, to all who want to learn about groundwater. In short, providing essential knowledge tools for developing groundwater sustainably for humanity and ecosystems.

This is a new type of global educational endeavor in that it is based on the volunteerism of professionals from different disciplines and includes academics, consultants and retirees. The GW-Project involves many hundreds of volunteers associated with more than 200 organizations from 27 countries and six continents, with growing participation.

The GW-Project is an ongoing endeavor and will continue with hundreds of books being published online over the coming years, first in English and then in other languages, for downloading wherever the Internet is available. An important tenet of the GW-Project books is a strong emphasis on visualization via clear illustrations that stimulate spatial and critical thinking to facilitate the absorption of information.

The GW-Project publications also include supporting materials such as videos, lectures, laboratory demonstrations, and learning tools in addition to providing, or linking to, public domain software for various groundwater applications supporting the educational process.

The GW-Project is a living entity, so subsequent editions of the books will be published from time to time. Users are invited to propose revisions.

We thank you for being part of the GW-Project Community. We hope to hear from you about your experience with using the books and related material. We welcome ideas and volunteers!

The Groundwater Project Steering Committee

June 2022

v

## Foreword

Groundwater science has advanced largely by measurements of parameters such as water pressure, temperature and salinity, in boreholes or wells or along the bottom of lakes and rivers. Well-established geophysical methods using electrical, electromagnetic, seismic, radar or temperature signals also contribute to understanding groundwater. These signals are collected using instruments located in airplanes, on the land surface or in boreholes.

This book is an introduction to a new field of geophysical technology that can be used in boreholes, or on the bottom of rivers or lakes to gain insight into the aquifer system. This method is known as Distributed Fiber Optic sensing where fibers are embedded in a cable to acquire measurements along the cable. The fibers are continuous strands of glass, each about the diameter of a human hair. The optical fiber is the core of a cable assemblage that can range from as small as less than 1mm diameter for shallow applications to several centimeters in diameter for deep ocean or geothermal-well installations. An apparatus (commonly referred to as an “interrogator”) connected to the cable sends and records the feedback of pulses of light (photons) along the fiber which are influenced by the temperature or the strain along the cable and in the surrounding aquifer. Hence, a continuous distribution of temperature, or strain, parameters are profiled along the cable. For example, in fractured rock, the temperature profiles over time identify the fractures with the most active groundwater flow.

For temperature, this is the equivalent of having an assemblage of many direct temperature measuring devices (e.g., thermistors) spaced at small intervals. However, the thermistors give point measurements with no data between the points and in contrast, the fiber optic cable provides values averaged over short segments of the cables and short time intervals. Typically, the distribution of temperature in groundwater is influenced substantially by groundwater flow, and by using fiber optics, the precision of the temperature values can be as small as a fraction of a degree Celsius. Therefore, the cables, which are relatively low in cost, can provide important insights into the flow conditions for which no other methods are practical. This technology has become well established in the petroleum industry over the past two decades. As the cost of the method is continually decreasing and its capabilities increase, these technologies are routinely used in research applications, and rapidly becoming common for routine aquifer monitoring. How this technology can serve groundwater science continues to expand.

The authors of this book are at the forefront of fiber optic research and have used the method in many types of applications in North America and Europe: Scott Tyler and John Selker are Professors at the University of Nevada, Reno and Oregon State University, respectively, while Tom Bogaard, Nick van de Giesen and Juan Aguilar-Bopez are professors at the Delft University of Technology, The Netherlands.

John Cherry, The Groundwater Project Leader  
Guelph, Ontario, Canada, June 2022

## Preface

This book focuses on the rapidly expanding field of fiber-optic-based distributed sensing with applications in hydrology and near-surface processes. While there are many texts and works devoted to fiber-based sensing, we strive in this text to provide the reader with an introduction to the technologies, a few examples and applications, and encouragement to apply some of these techniques. The potential for application to many other problems in hydrogeology and earth science is enormous, and our hope is that this text will inspire readers to dream.

## Acknowledgments

We deeply appreciate the thorough and useful reviews of and contributions to this book by the following individuals:

- ❖ Kamini Singha Professor, Hydrologic Science and Engineering Program; Dept. of Geology and Geological Engineering, Colorado School of Mines, USA;
- ❖ Miguel Gonzales, Researcher, Instituto Geológico y Minero de España, Spain;
- ❖ Luca Schenato, Professor, Electrical Engineering, University of Padova, Italy;
- ❖ Andrea Galtarossa, Full Professor, Electromagnetics, Department of Information Engineering, University of Padova, Italy;
- ❖ Dr. Jonathan Munn, Postdoctoral Fellow, Morwick G360 Groundwater Research Institute, University of Guelph, Canada;
- ❖ Everton de Oliveira, President of Hidroplan, Director-President of the Instituto Água Sustentável (Sustainable Water Institute), Brazil;
- ❖ Connie Bryson, Editor, The Groundwater Project, Canada;
- ❖ Matthys Dippenaar, Associate Professor, Engineering Geology and Hydrogeology, University of Pretoria, South Africa;
- ❖ John Greenhouse, Tobermory, Ontario, Canada;
- ❖ Carlos Maldaner, Research Scientist, Morwick G360 Groundwater Research Institute, University of Guelph, Canada;
- ❖ Beth Parker, Professor, School of Engineering, University of Guelph, Canada.

We appreciate the contributions of editor Kamini Singha, whose support, technical advice, friendship and most of all, patience through the process were greatly appreciated. We are grateful to Amanda Sills and the Formatting Team of the Groundwater Project for their oversight and copyediting of this book. We thank Eileen Poeter (Colorado School of Mines, Golden, Colorado, USA) for reviewing, editing, and producing this book.

Authors Tyler and Selker are grateful to the U.S. National Science Foundation for their continued support of the Centers for Transformative Environmental Monitoring Programs<sup>↗</sup> where many of the concepts and applications of fiber-based sensing in hydrology were born. Author Tyler also appreciates the community and NSF support of the Research Coordinating Network for Distributed Acoustic Sensing in Earth Sciences for the rapid advances in this new and exciting area.

# 1 Introduction

For the past several decades, earth scientists have been part of a sensing revolution. Driven by advances in miniaturization, computing power, solid-state physics and efficiencies in power requirements, almost every tool available to hydrogeologists has become smaller, faster, and more efficient. We can measure and retrieve data with higher resolution in space and time at a lower cost than ever before, allowing us to image and monitor the subsurface at ever finer and faster scales.

Still, many sensors including hydrogeophysical sensors, are essentially *point sensors*, which measure a quantity at a single point (or support volume). Only by distributing hundreds of sensors or making creative use of a limited number of sensors, such as in electric resistance tomography (ERT), can higher spatial resolution be obtained. This limitation is rapidly being erased by distributed sensing on optical fibers (e.g., Selker et al., 2006a; Tyler et al., 2009; Bense et al., 2016; Schenato, 2017). In hydrology, and most sciences, when it is possible to measure at higher spatial and temporal scales, the underlying processes, such as groundwater inflow into a stream, become much clearer.

*Distributed sensing* measures at sub-meter resolution on optical fibers and makes use of the continuously changing (in both space and time) properties of light transmission and scattering along tens of kilometers of optical fiber. While optical fibers have been used for decades for transmitting data and sensing at discrete points (where either the light within the fiber is directed outward, or where the light is directed through a sensor), continuous-in-space monitoring has only recently become possible and practical. In the next sections, we describe the theory, operation and example applications of distributed temperature, strain and strain rate applications in hydrogeology and hydrogeophysics. The book concludes with a few thoughts on the future and where it may take us.

## 2 Basic Principles of Fiber Sensing

Strategies for fiber optic sensing can be split into *sensitized fiber* and *intrinsic fiber* methods. An example of sensitized fiber is a *Fiber Bragg Grating* (FBG), used for decades for localized strain and temperature measurement within fibers. FBGs represent an “etched into fiber” sensor. Periodic changes in refractive index across a short length of fiber are made by engraving gratings into the fiber. As the fiber is strained through these sections, changes in the scattered light wavelength can be measured and related to the magnitude of strain by careful observation of the spectral backscatter that arises following insertion of a broad spectral pulse. FBGs represent “local” measurements and each point of measurement must have different grating spacings (to produce unique backscatter wavelength bands), which limits the number of FBGs that can be used on a single fiber to typically less than 200 (Hill and Meltz, 1997).

Unlike FBGs embedded in the fiber (analogous to individual electrodes in an electric resistance tomography string), intrinsic distributed sensing collects data throughout the length of the optical fiber, which can be many kilometers long. Optical fibers are designed to be highly transmissive to light which allows them to carry relatively weak signals over great distances. In principle, fibers are designed to be completely internally refracting for coherent light, obtained by layering glass of decreasing refractive indices from the inner “core” to the outer “cladding”. However, fibers are not 100 percent transparent, and some absorption of photons occurs.

Most distributed sensing relies upon scattering of laser-generated photons by interactions within the electrons of the silica ( $\text{SiO}_2$ ) molecules within the optical fiber. When photons are absorbed and re-emitted, a process commonly referred to as *scattered*, their scattering can take several forms. If the re-emitted photon remains at the same frequency and energy state as the absorbed one, the scattering is termed *elastic*. The most common elastic scattering is Rayleigh scattering, which is used in Distributed Acoustic Sensing (DAS). If, however, the re-emitted photon returns at a lower (or higher) energy state, the scattering is said to be *inelastic*. The magnitude of inelastic scattering and its impacts on the frequency and photon energy state can be used to infer the temperature and strain at the scattering location in the fiber. Common forms of scattering used in hydrogeophysical measurements are *Rayleigh*, *Raman* and *Brillouin scattering*. Figure 1 shows a typical spectrum of scattered photons in an optical fiber from an initially single wavelength energy source. When a scattering event occurs, the highest probability of scattering is elastic (Rayleigh). Raman inelastic scattering produces photons that fall into relatively narrow and predictable bandwidths, shifted in frequency either higher or lower. Brillouin scattering produces frequency shifts, and the frequency shift is a function of the strain at the scattering site.

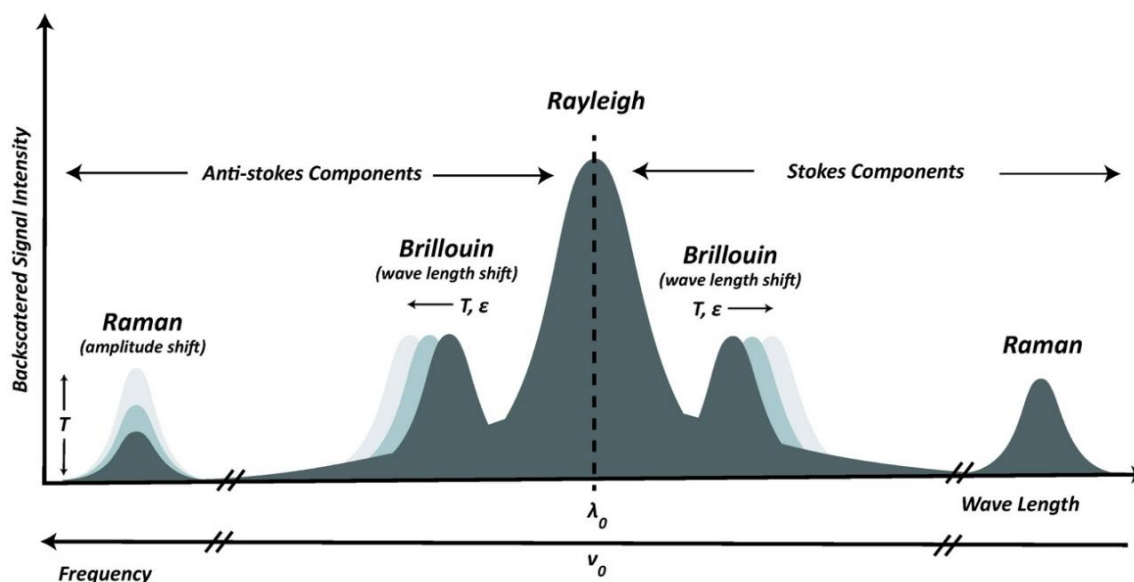


**Figure 1** - Diagram representing typical scattering intensity as a function of temperature  $T$ , wave length  $\lambda$  and strain  $\epsilon$  within an optical fiber. The incident wavelength is defined by the choice of laser and is typically in the near-infrared frequency (800-1500 nm), which is noted as  $\lambda_0$  near the center of the x axis. Raman scattering typically produces a scattered photon at predictable wavelengths of 20-100 nm both longer (Stokes) and shorter (anti-Stokes). The intensity of the shifted backscattered photons is used to estimate fiber temperature. Brillouin scattering employs density-dependent wavelength shifts, and it is the magnitude of the shift that corresponds to changes in glass density due either to a change in temperature or fiber strain.

The minimum length of fiber that returns a signal is a function of the maximum frequency of the detectors, the sensitivity of the detectors and the frequency of the laser repetition rate. The maximum length is constrained by the *optical budget* (the number of photons injected into a fiber) and the rate of scattering or attenuation of the photon numbers within the optical fiber. The intensity of injected light is limited by non-linear scattering properties which arise at high intensity. Some Distributed Temperature Sensing (DTS) instruments (commonly called “interrogators” in the industry) extend the range of these methods by sequentially injecting differing intensities wherein the highest intensity injections are only employed further from the point of injection to avoid non-linear effects while obtaining readings from greater distances.

Distributed sensing is now widely used for temperature measurement, strain measurement and, most recently, strain rate measurement. In hydrogeology, distributed sensing is widely applied for assessing surface water/groundwater interactions, soil moisture, groundwater flow, heat transport in the subsurface, strain and ground motion related to pumping, tides, and surface loadings. DAS is now poised to become standard practice in seismic refraction and reflection surveying.

Common to all distributed fiber sensing methods are: a low power laser illumination source (commonly in the near infrared), an optical fiber whose light transmission, scattering or length is a function of the property to be measured; and

detectors/processors to control the laser firing and to measure the returned light signal. Distributed sensing has many analogies to other remote sensing tools; it is most closely related to lidar (light detection and ranging) where scattering photons from interactions with the land surface are recorded and their time of flight is used to calculate the distance from the laser source to the scattering site.

### 3 Fiber-Optic Distributed Temperature Sensing (DTS)

Heat transport in the subsurface is an important phenomenon for many hydrogeologic processes, ranging from the shallow vadose zone to the deep geologic disposal of nuclear waste. Heat transfer is usually calculated from measured temperatures or temperature fluctuations in boreholes or soils, using point sensors such as thermistors and thermocouples. These can have very high accuracies (0.001 °C) and precision (+/- 0.0001 °C).

DTS allows the inference of an optical fiber's temperature at decimeter to meter resolution, depending on the design of the interrogator. DTS relies upon Raman scattering (where a photon is absorbed, and then a new photon is emitted, what is referred to as inelastic scattering) to infer the temperature of the material that re-emitted the photon. When a photon is absorbed and re-emitted from a Raman scattering event, the re-emitted photon will be frequency shifted either to a fixed lower frequency (termed a *Stokes photon*) or to a fixed higher frequency (termed an *anti-Stokes photon*) as shown in Figure 1. The probability of re-emitting an anti-Stokes photon increases as the scattering site temperature increases, thus the ratio of anti-Stokes to Stokes intensities in the backscatter can reveal the temperature of the location where the scattering took place. In operation, a short (multiple nanoseconds) pulse of laser light is sent down the optical fiber and, while most of the injected photons pass through the optical fiber without interacting with the fiber's glass, some photons will undergo Raman scattering. A portion of these Raman photons will be emitted such that they are internally refracted and travel back up the optical fiber to the laser source. Upon entering the instrument, they are diverted to detectors tuned to the typical frequency shift of Raman scattering in fiber where they are counted electronically. The distance of the scattering event from the laser source is calculated from the known speed of light in the optical fiber, and the time of flight since the laser was pulsed. Photons are counted until the time of flight exceeds the known total length of the fiber. After this time, another pulse is sent down the fiber, and the process is repeated. Photons are accumulated and, analogous to seismic reflection, tens of thousands of these signals are accumulated or "stacked" to increase the signal-to-noise ratio.

The fiber length associated with each scattering event commonly termed *sample spacing* is a function of the pulse time of the laser and the speed at which the detectors can function (Tyler et al., 2009). For a 10-nanosecond laser pulse time, photons will travel ~2 m. If the detectors collect backscattered photons during the first 10 nanoseconds after the pulse is launched, these scattering events must have occurred in the first meter of the fiber.

DTS minimum *spatial sampling or sampling interval* is defined as the shortest spatial distance between successive *reported* Stokes and anti-Stokes measurements and is controlled by the instrument's frequency of laser firing and the minimum sampling time

for the instrument's Stokes and anti-Stokes detectors. DTS is typically operated at the minimum sample spacing supported by the instrument manufacturer. But it is very important to understand that DTS reported temperatures of adjacent samples are not fully independent. For this reason, a *spatial resolution* (a performance metric for an instrument) is also specified to indicate how proximal temperature features may be distinguished and quantified. From Nyquist (1928) we know that *spatial resolution* is universally at least two times larger than the *sample spacing*, but in the case of DTS machines, these are sometimes different by as much as a factor of 10. Instrument performance as specified by its spatial resolution is typically defined as the distance between points located at 10 percent and 90 percent of the total temperature, the true temperature change at a stepwise shift in temperature along a fiber optic cable. In other words, the distance between points surrounding a sharp temperature change such that the point on the low side is not elevated by more than 10 percent of the jump and the point on the high side is elevated by at least 90 percent of the actual.

Because of dispersion of light along fiber optics, finite time for lasers to turn on and off, and limitations of optical detectors and their amplifiers to respond to changing signals, reported DTS temperatures are weighted sums of the temperatures along a cable. Laboratory tests on several systems have indicated that the weighting function is typically Gaussian, which is reasonable considering the nature of these systems. This implies that the reported value for a point  $x$  is the weighted sum of the unit Gaussian with standard deviation  $\sigma$  centered at  $x$  multiplied by the actual temperatures along the cable (Figure 2).

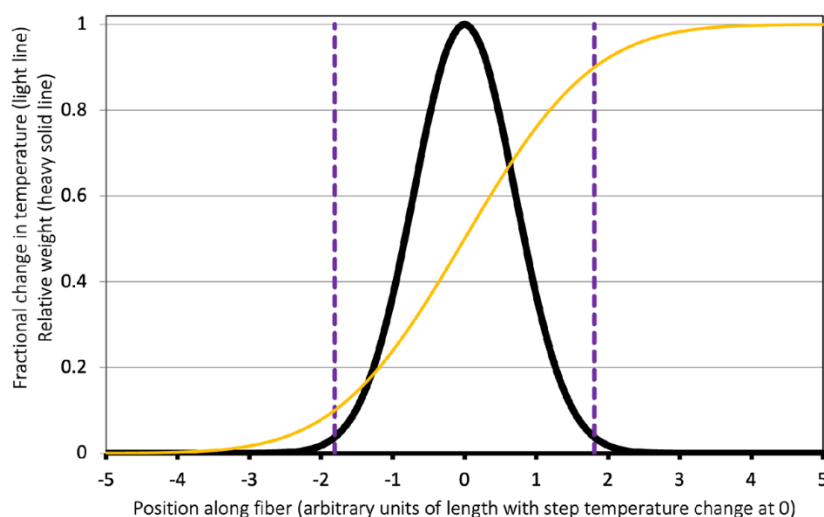


**Figure 2** - Gaussian curve with a maximum of 1 and standard deviation ( $\sigma$ ) of 1 illustrating the weighting function implicit in the 10-90 definition of DTS spatial resolution. The yellow solid line presents the reported DTS temperatures, the heavy solid black line the Gaussian weighting function over which the DTS averages in its reported temperature at position 0, and the dashed lines indicate the locations along the cable of the 10 percent and 90 percent quantiles of change in reported temperature where the true temperature change occurred at position 0 on the horizontal axis.

Selker and others (2014) explored these issues in the context of the work done by Rose and others (2013), where data were collected with a 2-m resolution DTS and sections of cable far smaller than 2 m were exposed to local heating. In general, the physics underlying DTS is very robust and worthy of study for those employing this method. For example, a DTS system must assume a certain speed of light of the original pulse and of the Stokes and anti-Stokes wavelengths. The exact speeds will depend on the exact make of optical fiber. A small deviation between actual and assumed speeds of less than 1 percent quickly leads to “dislocations” at distances of hundreds or thousands of meters along the fibers. Further discrepancy between DTS-reported position and the distance along a cable is caused by “over-stuffing” of the fiber in the cable wherein the fiber optic is longer than the cable (typically on the order of 0.3 percent or less). This is done so that if the cable experiences tension and is stretched slightly, the fiber will not experience tension. If accurate location is important, it is good practice to verify measured distances in the field by temporarily heating (or cooling) a small section of the cable. Similarly, it often pays to work directly with the measured Stokes and anti-Stokes signals instead of the temperatures calculated within the instrument using default calibration parameters. Because the DTS signals travel at different velocities and are affected differently by irregularities such as splices or acute bends (broadly referred to as differential attenuation), the raw Stokes and anti-Stokes values can be post-processed to provide a more accurate temperature.

The calculation of fiber temperature fundamentally relies upon the increasing probability of anti-Stokes interactions as the fiber temperature warms. This probability follows a Boltzmann distribution with the distribution’s exponent controlled by the scattering temperature. In practice, the Stokes and anti-Stokes photon counts are each integrated to an intensity term,  $I_s$  and  $I_{as}$  respectively. Additionally, the overall magnitude of scattering or attenuation for both the Stokes and anti-Stokes frequencies is required to correct for the ever-decreasing number of photons available for scattering the further along the length of the optical fiber,  $z$ .

A key point here is that the greater scattering of the anti-Stokes at any location means that the rate of attenuation of light is quite different for the Stokes and anti-Stokes signals due to their different colors (wavelengths). The less-scattered red-light travels in a straight line, just as at sunset when red light is seen on the horizon while the sky directly above looks blue because the blue light from the sun is scattered towards us. Because we infer temperature from the ratio of anti-Stokes to Stokes, we must correct for the change in this ratio due to losses that occur from the location of the scattering event to the detector in the instrument. Similarly, bends and other defects in the fiber will cause different levels of attenuation of the two wavelengths. In summary, attenuation may vary along the fiber, due to manufacturing, defects, bends or connections. This difference in attenuation, usually denoted as  $\Delta\alpha(z)$ , for the two returning signals can be written as a cumulative integral that adds up all the differences in attenuation encountered along the optical path. The

temperature ( $T$ ) of the sample length can be derived (van de Giesen et al., 2012) as shown in Equation 1.

$$T\left(z, \frac{I_s}{I_{as}}\right) = \frac{\frac{\hbar\Omega}{k}}{\ln\left(\frac{C_s}{C_{as}} \frac{\lambda_s^4}{\lambda_{as}^4}\right) - \int_0^z \Delta\alpha dz + \ln\left(\frac{I_s}{I_{as}}\right)} \quad (1)$$

where:

$I_s$  = measured photon intensity of Stokes ( $\text{MT}^{-3}$  or  $\text{ML}^2\text{T}^{-3}$ )

$I_{as}$  = measured photon intensity of anti-Stokes ( $\text{MT}^{-3}$  or  $\text{ML}^2\text{T}^{-3}$ )

$z$  = distance along the optical fiber (L)

$\Delta\alpha$  = difference in attenuation factors between Stokes and anti-Stokes ( $\text{L}^{-1}$ )

$\hbar$  = reduced Planck's constant ( $\text{ML}^2\text{T}^{-1}$ )

$\Omega$  = frequency difference between Stokes and anti-Stokes scattering in typical fiber ( $\text{T}^{-1}$ )

$k$  = Boltzmann constant ( $\text{ML}^2\text{T}^{-2}\Theta^{-1}$ )

$c_s$  and  $c_{as}$  = Constants related to laser power and responsiveness of the DTS detectors ( $\text{MT}^{-3}$  or  $\text{ML}^2\text{T}^{-2}$ )

$\lambda_s$  and  $\lambda_{as}$  = wavelengths of the Raman shifted returning light (L) as discussed by Farahani and Gogolla (1999)

In common DTS discussions, the numerator of Equation 1 is made up of constants and is routinely shortened as  $\gamma$  and the first term of the denominator is replaced by a single variable,  $C$ . Equation 1 can be further simplified to Equation 2 if it is assumed that the difference in attenuation properties for the Stokes and anti-Stokes photons,  $\Delta\alpha$ , is constant along the length of the fiber (Hausner et al., 2011).

$$T\left(z, \frac{I_s}{I_{as}}\right) = \frac{\gamma}{C - \Delta\alpha z + \ln\left(\frac{I_s}{I_{as}}\right)} \quad (2)$$

As there are now several coefficients in Equation 2, it is generally necessary to have several independent temperature sensors along the length of the cable, serving as calibration points, to estimate these coefficients. These calibration points typically consist of a section of the measuring cable of a minimum length of 10 times that of the sample interval whose temperature is unchanging during each DTS measurement time. For example, ice baths or well-stirred insulated containers can be used to maintain a sufficient length of cable at a constant temperature.

It is common to construct cables to have multiple optical fibers. The first reason for this is that adding extra fibers does not add much cost to most cables. An example of a typical fiber-optic cable is shown in Figure 3. Multimode fibers allow multiple optical paths

within the core and, while generally having greater attenuation, multimode fibers are commonly used for temperature sensing. Single-mode fiber allows only one “mode” of the light wave to propagate down the fiber, with fewer refraction events per unit distance and less attenuation. Single-mode fiber is typically used for distributed acoustic sensing or very long (> 20 km) DTS installations. Cables can also have a wide range of construction elements but generally, all consist of fiber(s) as well as various strength elements and plastic jacketing material.

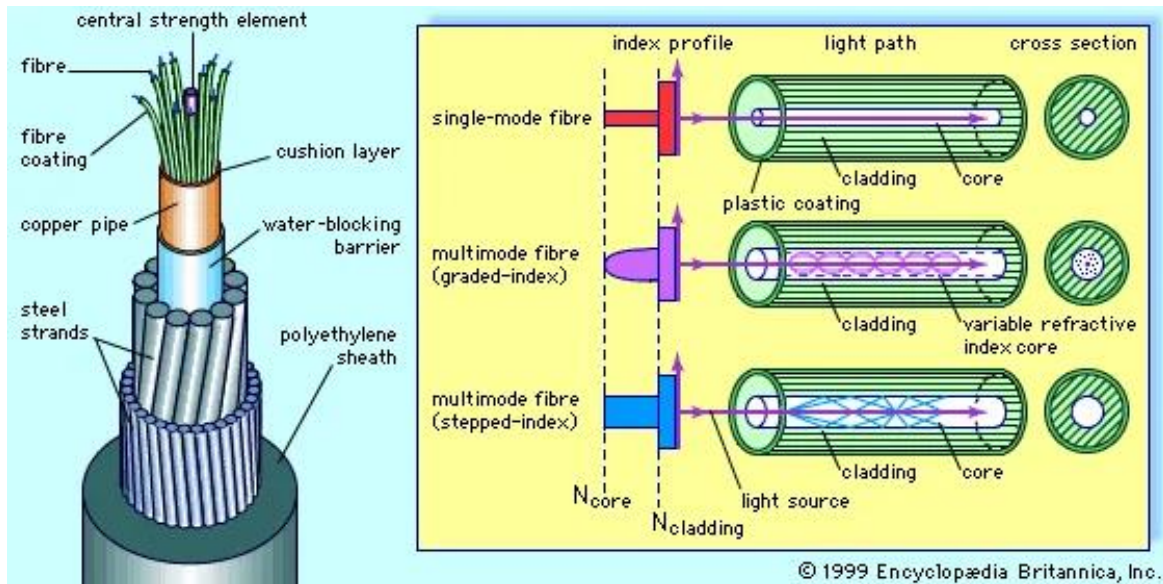


**Figure 3** - Schematic of common fiber-optic cable design. Here, the fibers are encased in a metal tube (in this case copper but more commonly stainless steel). The right side of the figure conceptually shows the difference between single-mode fiber and multimode fiber, along with the differences in the nature of the interface between the two different glasses of the core and cladding glass (from Encyclopedia Britannica).

“Bare” fibers cost ~US\$ 0.05/m, while a fully constructed cable typically costs US\$1-10/m. Installation is much more expensive per meter than the bare fiber, so it is highly recommended that at least two multi-mode and two single-mode fibers be included in any installation. This allows for more options and redundancy of the installation. One option is obtained by connecting two of these fibers at the cable’s distal end (or by looping the cable back to the instrument and connecting both ends of the fiber to the instrument), in which case the fiber is said to be in *duplex* mode. By interrogating in both directions and combining these signals, it is possible to calculate the spatial distribution of the differential attenuation directly and reduce the calibration parameters and calibration points to a single independent measurement (van de Giesen, 2012; des Tombe et al., 2019; des Tombe et al., 2020; Ghafoori et al., 2020).

Putting this into a larger context, it is useful to review the basic topologies for DTS cable and calibration systems, ranging from a single strand of fiber (simplex) to a looped or double fiber configuration (duplex) as shown in Figure 4. Once the geometry of the fiber is

decided, the user then can decide to interrogate each fiber separately (single-ended measurement) or combine the signals from both fibers (double-ended measurement). There are pros and cons to each of these approaches. Single-ended measurements become noisier the further away from the source but require more calibration points; double-ended measurements have more noise close to the source, (Hausner et al., 2011, van de Giesen et al. 2012, des Tombe et al., 2020; Ghafoori et al., 2020).

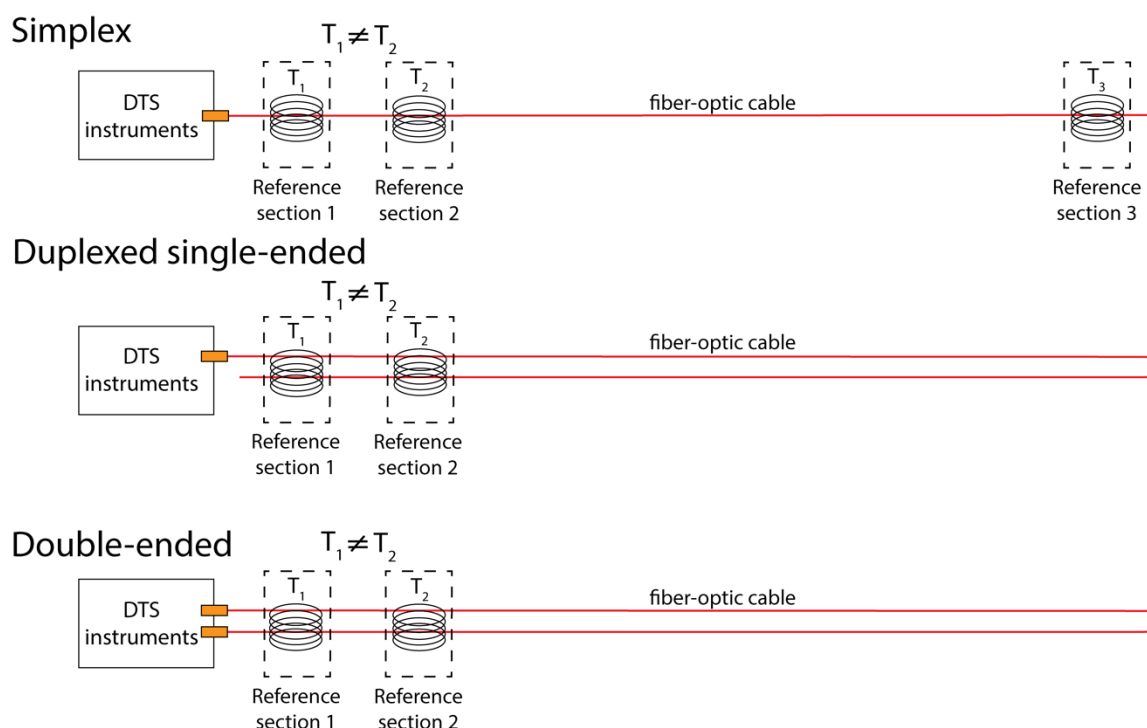


**Figure 4** - The three most common DTS fiber configurations. A single-ended measurement sends light in only one direction down the fiber, while double-ended measurements require that light be sent in both directions. Double-ended measurements require that the DTS system have at least two separate channels for fiber connection. The coiled cables in the diagram represent at least 10 measurement points on the fiber that are kept at a constant temperature.

A key consideration in designing a cable layout is the calibration and validation of the signals. First, estimating the spatial distribution of the differential attenuation,  $\Delta\alpha$ , requires that calibration points are spaced *along* the fiber. Determination of the other two calibration parameters in Equation 2 requires two distinct zones of different temperature, all together this provides three equations to solve for these three terms.

An example set of DTS signals (or traces) are shown in Figure 5. In this example, a ~300 m singled-ended fiber had been deployed at the snow/soil interface across an area of approximately 0.5 hectares or 5000 m<sup>2</sup> (Tyler et al., 2009). At the time of this measurement, most of the fiber was buried beneath ~1 m of snow, however, some areas had melted and the fiber ran across bare, dark volcanic soil.

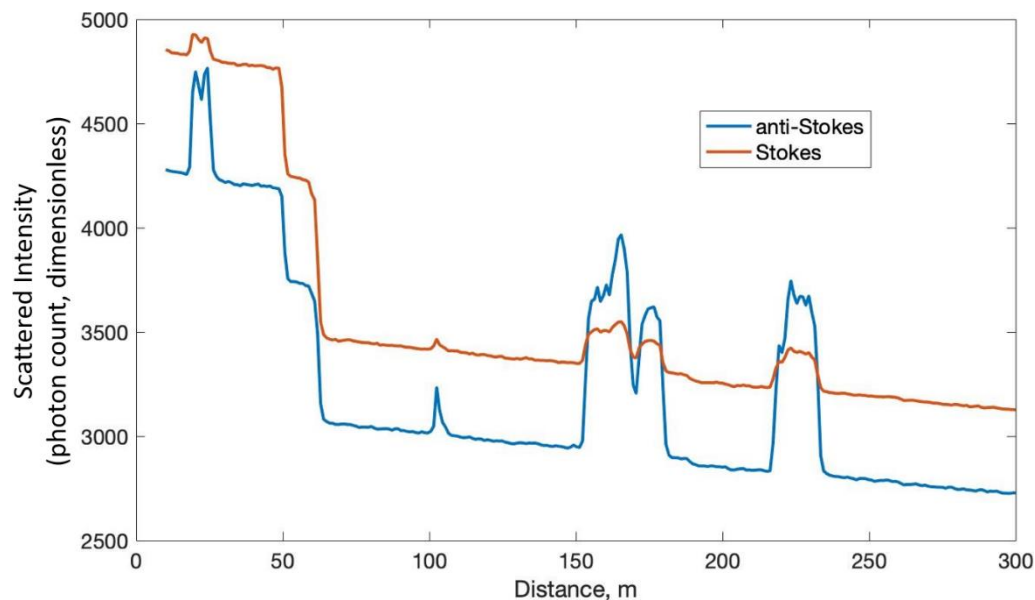


**Figure 5** - Typical DTS trace from a ~300 m long fiber partially buried beneath snow. The large positive excursions in the anti-Stokes signal represent areas where the fiber was not buried under snow and exposed to direct sunlight. The sudden drops in both Stokes and anti-Stokes amplitude from 40 to 60 m are “step losses” resulting from strain on the fiber caused by sharp bending of the fiber around trees and over rocks.

Several important features common to DTS data are shown in this figure. The large positive excursions of the anti-Stokes (and to a much lesser degree, the Stokes return) represent areas where the fiber was exposed to direct sun and was warmed far above the temperature of adjacent fiber buried beneath the snow. Both the Stokes and anti-Stokes magnitude slowly decline with distance from the DTS, resulting from the loss of photons by scattering along the fiber. While this slope appears linear in Figure 5, it follows Beer’s Law of attenuation, which plots linearly on a semi-log graph. In this case, the exponential attenuation coefficient is very small resulting in a visually linear slope. Beer’s Law implies that the attenuation (or scattering of light) will follow an exponential decline with distance. Several sharp declines or downward steps in both Stokes and anti-Stokes return can be seen between 40 and 60 m from the start. These are commonly termed *step losses* and result from localized increases in the attenuation of light. This can be caused by simply bending the fiber such that the internal refraction is no longer sufficient to constrain the light, by microcracks or other strain, and wherever the light must pass through a mechanical connection or repair of the fiber. In Figure 5, most of the steps were caused by the fiber bending around trees and over sharp rocks, resulting in tight bends in the fiber.

### 3.1 DTS Applications in Hydrogeology

By the 1990s, DTS was used primarily in the oil and gas industry for monitoring steam flooding in heavy oil reservoirs and monitoring temperature anomalies in high voltage electric transmission lines. The paper by Shanafield and others (2018) documents

the transition of DTS (and other fiber-based tools) from industrial to hydrologic acceptance. Hydrologic applications began in the late 1990s with monitoring of seepage in dams (Weiss, 2012; Johansson, 1997; Johansson and Sjö Dahl, 2004; Johansson and Sjö Dahl, 2007). By using the seasonal change in reservoir temperature as an upstream boundary condition, Johansson (1997) matched the thermal evolution of the dam fill material (as measured by a buried optical fiber) to predictions from the thermal advection-conduction equation to estimate the magnitude of additional heat transport due to seepage (advection). Under non-seeping conditions, the seasonal heating and cooling of the reservoir water produces a roughly sinusoidal conductive heat pulse horizontally through the dam material. Where seepage is present, the heat pulse is accelerated due to advection. This approach is now widely used for dams and earth-filled levees to detect seepage (Johansson and Sjö Dahl, 2007). The method is most appropriate for high latitude regions, where a strong seasonal variation in water body temperature can be assumed.

Significant growth in the use of DTS for hydrology and hydrogeology was driven in large part by the work of Selker and others (2006a, b), who demonstrated its significance in the analysis of groundwater/surface water interactions. Already an emerging topic in the early 2000s, the understanding and quantification of hyporheic flows (the exchange between surface waters and groundwaters) was hampered by the lack of high-resolution spatial measurements. Integrated tracer testing (Bencala et al., 2000) provided bulk exchange measurements; vertical measurements of point-scale temperature in the streambed (Constanz et al., 1998) offered only a glimpse of the local exchange processes. By monitoring streambed temperature along a 1.4 km reach of stream in Luxembourg at spatial scales of ~1 m and at time scales of ~1 minute, Selker and others (2006b) were able to map numerous groundwater inflows (Figure 6).

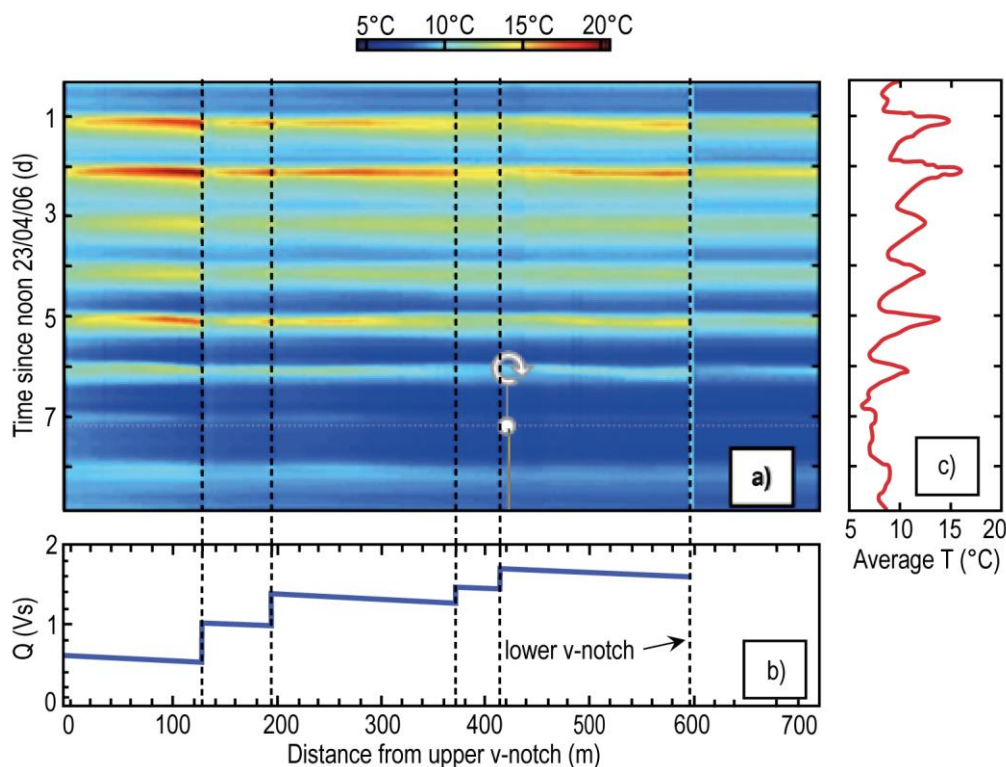


**Figure 6** - a) Stream temperature in time and space from April 24 to May 3, 2006, for the first 720 m of the Maisbich in Luxembourg; b) computed stream flow with groundwater inflows at the dashed lines computed from temperature measurements, and up and downstream flow obtained from weirs; and, c) time-series of spatially averaged temperatures. The first two days (April 24 and 25) were sunny, while the last two days (April 30 and May 1) were cloudy (from Selker et al., 2006b, with permission).

Mapping the inflow of groundwater to streams was a significant advance, although this type of data could in principle be gathered from a time-consuming synoptic temperature survey using a handheld thermometer. Of more significance, however, was the use of the time-varying streambed temperature to directly calculate the volumetric flux of groundwater to the stream. Because the stream temperature had a strong 24-hour or “diel” signature, points of groundwater inflow cooled the stream during the late afternoon but warmed the water downstream during the early morning. By noting the point in time when groundwater neither warmed nor cooled downstream, the observed temperature at that point in time and space represented the true groundwater temperature, a measurement that was rarely made. Armed with this information, it was then possible to calculate, from a thermal balance model, the actual volumetric flux of groundwater entering the stream at each of these points, a measurement that could not be made with sufficient accuracy from standard stream gauging (Selker et al., 2006b; Westhoff et al., 2007). The measurement of exchange between surface waters and groundwaters continues to advance and evolve significantly with work in estuaries (Henderson et al., 2009), high-resolution vertical DTS profiling (Briggs et al., 2012), exchange in lakes (Blume et al., 2013), seepage and slope

failure (Bersin et al., 2017; Schenato, 2017; Weiss, 2012; Perzimaier et al., 2007; Wu et al., 2019), and groundwater-recharge basins (Medina et al., 2020).

DTS is also now widely used to measure vadose zone processes by burying optical fiber and monitoring its temperature in response to daily/seasonal heating, or by actively heating the fiber and monitoring its thermal response (e.g., Sayde et al., 2010; Benitez-Buelga et al., 2014; He et al., 2018). In the case of daily or seasonal response, the primary variables affecting the thermal response are the rates of seepage (advective heat transport) and the soil thermal properties (primarily conductive heat transport, principally governed by the soil water content).

Work on seepage through dams and embankments relies upon the perturbation from a daily or seasonal conductive-only temperature time series. The magnitude of the advective perturbation is a function of the seepage or infiltration flux. For example, several authors (Gregory, 2009; Medina et al., 2020) calculated seepage fluxes across a large infiltration basin documenting significant spatial variability in flux rates, but also the evolution over time of the clogging of the spreading basin. Such hydraulic engineering applications of DTS continue to expand and installation of monitoring fiber is now common practice for many new dams, levees, and infiltration basins.

Developing high-resolution (both time and space) soil-moisture mapping represents a fundamental challenge in vadose zone hydrology. Most measurements are either point measurements, (measuring a volume of a few cubic centimeters), depth limited (microwave methods limited to the first 5 to 10 cm of the soil surface) or integrated sensors such as COSMOs (Cosmic-ray Soil Moisture Observing System) capable of integrating over tens of meters. By burying optical fiber, very high spatial resolution measurements can be repeatedly made. In their paper, Steele-Dunne and others (2010) first proposed to use multiple fibers, buried at varying depths, to infer soil thermal diffusivity from the phase and amplitude of daily temperature variations driven by solar heating. Soil thermal diffusivity,  $D$ , can be written as Equation 3.

$$D(\theta) = \lambda(\theta) / \rho Cp(\theta) \quad (3)$$

where:

$\theta$  = soil volumetric water content (dimensionless)

$\lambda(\theta)$  = soil thermal conductivity ( $\text{ML}^1\text{T}^{-3}\theta^{-1}$ )

$Cp(\theta)$  = soil heat capacity ( $\text{ML}^2\text{T}^{-2}\theta^{-1}$ )

$\rho$  = water density ( $\text{ML}^{-3}$ )

Under the assumption that soil water content,  $\theta$ , was the only soil property to be changing over time, the authors showed that soil moisture evolution could be mapped over time by estimating the soil thermal diffusivity. A publication by Dong and others (2016)

improved the sensitivity of the approach by incorporating a Richard's equation solution to improve the water content estimation resolution.

Because the soil thermal diffusivity is only weakly a function of soil water content and is also not monotonic in water content, Sayde and others (2010) adapted the soil heat-pulse sensing concept to optical fiber design. When a constant heat flux is applied to an optical fiber (typically through a distributed resistance heating element), its rate of heating is primarily a function of the soil thermal conductivity rather than the soil thermal diffusivity. Thermal conductivity is controlled by the soil-particle conductivity, soil water content and air content. The bulk soil thermal conductivity is generally linearly related to soil water content (excluding the very dry and very wet end of the soil water spectrum), and therefore any changes in time to the thermal conductivity will likely reflect changes in soil water content under the assumption that other soil properties such as dry bulk density do not significantly change over time.

Sayde and others (2010) incorporated resistance heating using the metallic armoring of an optical fiber cable and under modest rates of heating (10 W/m) noted that the cumulative heating (analogous to the total heat transfer) was strongly related to the volumetric water content (Figure 7). The relationship between water content and heating is consistent with the decrease in thermal conductivity with decreasing water content.

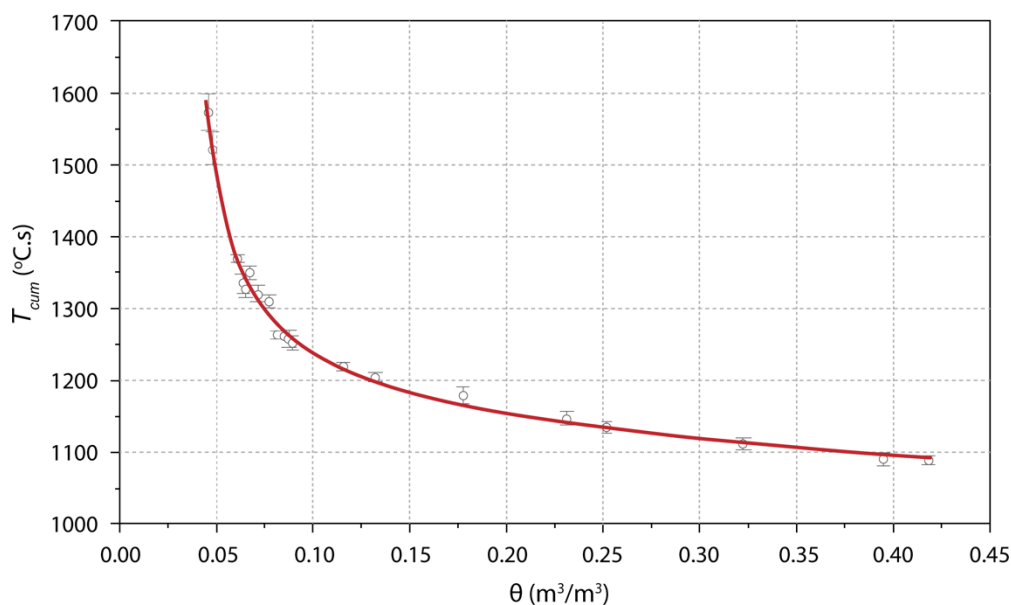


**Figure 7** - The relationship between soil volumetric water content,  $\theta$  and the cumulative increase in fiber temperature,  $T_{cum}$  for a 120-second heat pulse (with permission from Sayde et al., 2010).

Active heating of fibers in the vadose zone continues to be an evolving and very promising technique. Improvements in heating control, power requirements and analysis continue to be made (for example, as shown by Sayde et al., 2014; Ciocca et al., 2012;

Sourbeer and Loheide, 2015; Dong et al., 2017; Abesser et al., 2020; and Simon et al., 2020), and as discussed next, active heating also has applications below the water table.

In a definitive article, published in 2020, on the application of active heating to cables embedded in porous media, Simon and others explored the entire parameter space surrounding the rate and duration of heat delivery, the thermal properties of the porous media, and the rate of water flow (Figure 8). It became apparent that for advection to be the dominant control of measured temperature, groundwater flux must exceed about 0.1 m/d, and to detect such a low flux rate, heating must be carried out for more than a full day. For groundwater fluxes in the 1 m/d range, heating can be as short as 4 hours, and for 5 m/d, as little as 15 minutes, using an injected energy of 20 W/m along the cable.

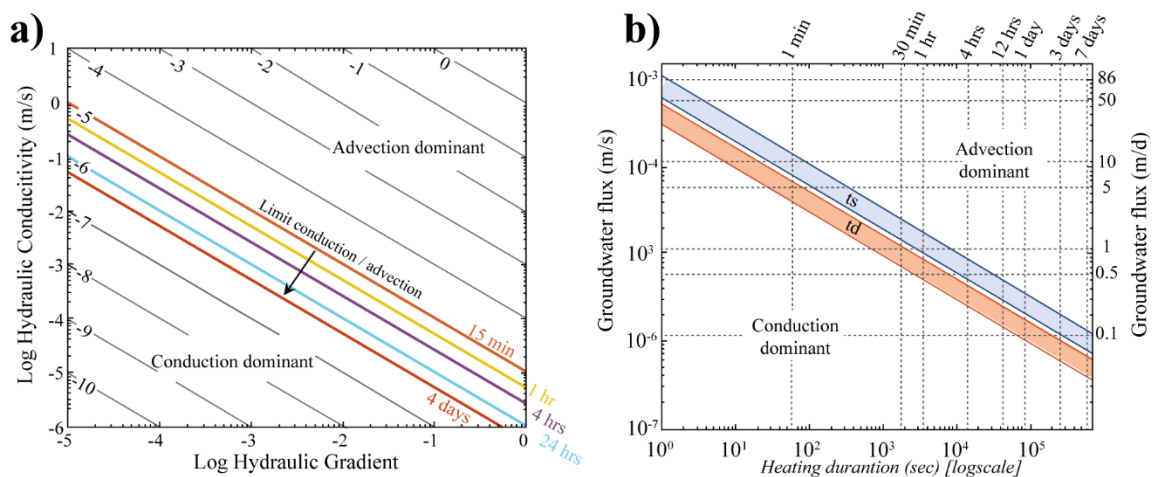


**Figure 8** - a) Transition between conductive and convective heat transfer as a function of the hydraulic gradient and hydraulic conductivity (fluid velocity) and its relation to heating times of an actively heated cable. b) Heating duration versus groundwater flux.

Below the water table, DTS has been widely used to monitor thermal gradients and cross-formation flow within boreholes in thermal tracer tests (Bense et al., 2016) and monitoring ground-source geothermal systems (McDaniel et al., 2017). Bakker and others (2015) as well as des Tombe and others (2019) developed a direct-push drill system capable of simultaneously installing a loop of optical fiber for monitoring thermal tracer tests in soft sediments.

Thermal tracer tests, both short term and longer term, are optimal environments for DTS monitoring, as downhole sensor reliability is greater than traditional temperature loggers over long periods. Researchers have deployed fiber in several fractured rock boreholes and utilized both inert and thermally reactive tracers (as well as heat) to assess fracture connectivity (Hawkins et al., 2017; Banks et al., 2014). Figure 9 shows the general concept of an injection test in fractured rock, where the tracer, which could be heat, is advected through the borehole in permeable fractures.

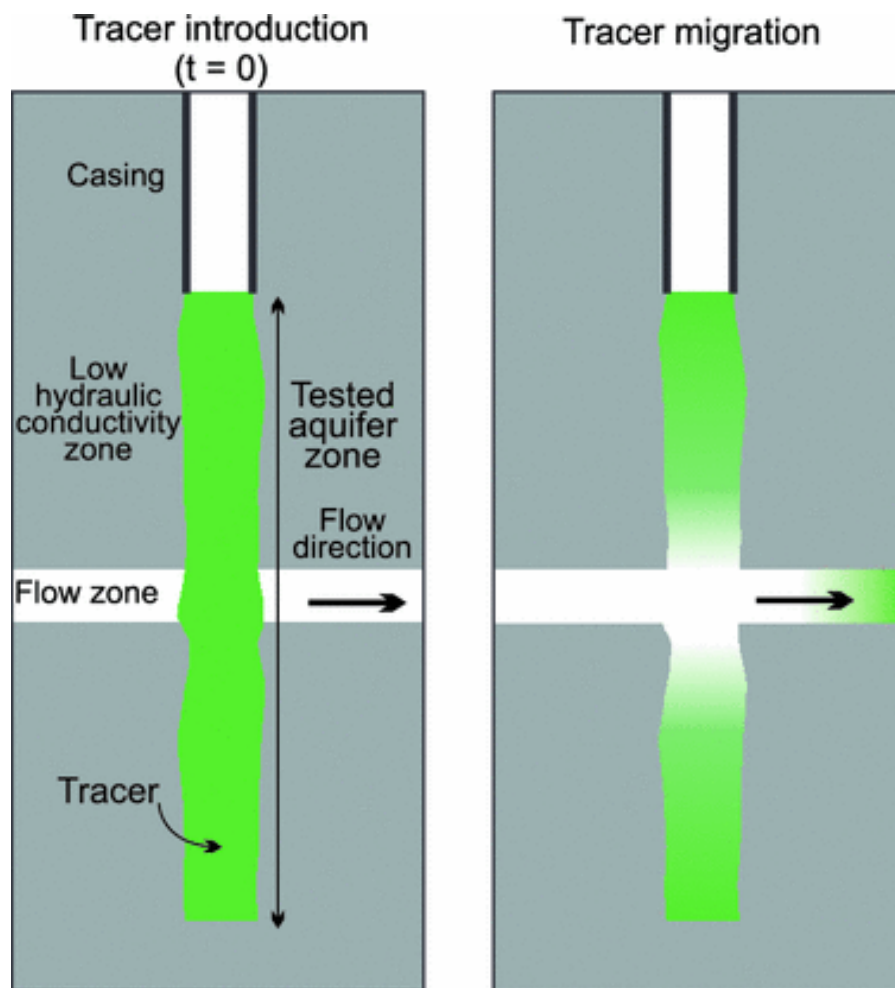


**Figure 9** - Conceptual transport of a tracer, either chemical or heat, initially injected into a borehole. The tracer is rapidly removed from the borehole in the vicinity of permeable horizontal fractures. For typical DTS applications, the tracer would be warmer water and the fractures would be delineated in the borehole DTS fiber by a localized drop in temperature over time that is more rapid than would be predicted by simple heat conduction.

Others have combined borehole heating with temperature monitoring to both estimate aquifer thermal properties in cased boreholes and horizontal fluid flux through screened intervals of the boreholes (Hausner et al., 2016). In a novel and greatly expanded use of DTS, McDaniel and others (2017) installed DTS fiber in 2,596 boreholes within and surrounding a geothermal heat exchange wellfield in Wisconsin, USA, to monitor and improve the energy efficiency of heat injection/extraction. Leaf and others (2012) conducted open-hole thermal testing; by simply injecting warm water at various depths in an open borehole. Natural flow direction in the borehole was easily measured, as was uptake into fractures. While buoyancy effects complicated the analysis, borehole flow was often downward overcoming buoyancy. Use of DTS for flow logging in wells is now well developed (Read et al., 2014; Read et al., 2015), in which a point heat source is used to inject a heat pulse into a borehole, and its dilution from inflows during heating can be mapped

vertically, documenting zones of inflow to the well. Selker and Selker (2018) added the concept of heating a vertically oriented cable at discrete locations wherein the resulting heat pulses could be tracked vertically along the fiber to allow detection of both horizontal and vertical water flow.

A key challenge to borehole applications of DTS is the free advection of water within the well. Klepikova and others (2018) showed advection could be eliminated by adding 0.1 percent polyacrylamide (PAM) gel to the water in a well. This provides for a “temporary grout” of the cable so that the data reflect the aquifer characteristics rather than the movement of water within the well. Since PAM gel is soft, instruments can easily be moved through the gel as needed to take local water samples/measurements or to carry out injections of water or electrical current for tomographic studies. Following use, the PAM can be removed by slowly pumping the well.

In most of the cases described above, DTS measurements are only observing a heated or natural flow system and the actual heat transfer from the fiber is not used to infer aquifer properties. With active soil-moisture monitoring, the heat dissipation (or rise) rate from the fiber itself can be used to infer aquifer thermal properties and fluid velocities. DTS is now widely used in an active mode, in which the fiber and cable elements are heated at a known rate of heat input, and the thermal rise or decay of the temperature at the fiber and cable are used to infer aquifer or seepage properties through dams and levees (Perzmaier et al., 2004, Bakx et al., 2019). As with active soil-moisture monitoring, a resistive heating element is incorporated in the cable system that contains one or more optical fibers. Here we depart slightly from the terminology of Bense and others, (2016) as we define active DTS in boreholes as tests that estimate aquifer properties based on heat transfer from the DTS cable to the formation or fluid, rather than heating of either the borehole fluid or rock mass and monitoring its temperature. Freifeld and others (2008) were the first to actively heat fiber in deep boreholes to estimate the vertical variation of thermal conductivity. By numerically inverting the response, the authors estimated the vertical variation of the thermal conductivity, for later use in reconstructing paleosurface temperature.

Other researchers utilized a heated-fiber system installed between the formation and a flexible borehole liner (Coleman et al., 2015; Maldaner et al., 2019). The liner reduces or eliminates vertical flow within the borehole and allows for measurement under natural hydraulic gradients. The flexible liner allows the borehole to be used for other purposes after DTS testing, similar to the use of PAM gel as discussed previously (Klepikova et al., 2018) and can be extracted after testing.

While most actively heated fibers experiments strove for uniformly heating the fiber, Selker and others (2018) constructed a spatially variable heated fiber by tightly wrapping copper heating cable at 2-meter intervals along a fiber sensing cable. This

produced a higher heat flux in the tightly wrapped sections (~0.5 m) than in the remaining 1.5 m intervals where the heating cable was colinear with the sensing fiber (Figure 10). Using such a design allows for measurement of vertical fluid flow at numerous depths in a borehole and increases the practical length of cable that can be heated.

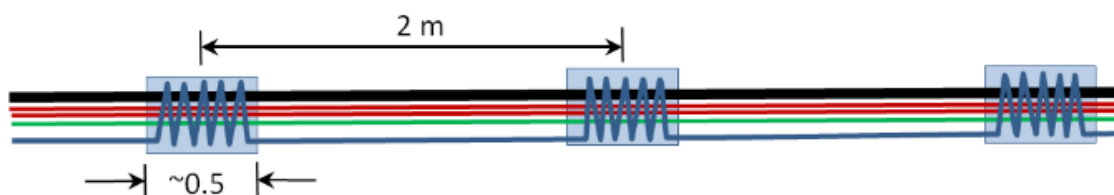


**Figure 10** - Schematic of a spatially variable heated optical fiber. Wrapping of the heater cable (shown in blue) produced heating “dots” that allowed for identification of vertical flow direction and magnitude at discrete depths within the borehole.

## 4 Strain Measurement

Strain, or the relative deformation due to loading, is an important hydrogeologic process. Vertical strain due to pumping in a well is a foundation of the concept of specific storage, and the field of geomechanics has taken on greater importance in the fields of geodesy and seismology in recent years as we recognize the relationships between fluids, fluid pressures and large-scale earth motions. Localized strain can be measured with a wide variety of sensors, ranging from load cells to GPS, but are typically point measurements. Distributed strain sensing on optical fibers has been evolving over the past several decades and is now well established in landslide monitoring although mainly focused on borehole sensing, pile monitoring, crack meters for rock instability and monitoring of retaining walls (Schenato, 2017). On the contrary, monitoring of the spatial distribution of surface displacement has seen only a few proof-of-concept experiments.

### 4.1 Brillouin Distributed Strain Sensing (BDSS)

Several different scattering principles can be used to measure strain (Kishida et al., 2014). Brillouin scattering, the inelastic scattering phenomenon described earlier, is the most common and is based on the principle that longitudinal strain (in the direction of the fiber) will produce a scattered photon whose frequency is shifted from the incident photon in linear proportion to the change in strain at the scattering site and the change in temperature at the site. From Zhang and others (2020), this can be expressed as Equation 4.

$$\Delta\nu_B = C_e\Delta\varepsilon + C_T\Delta T \quad (4)$$

where:

$\Delta\nu_B$  = change in Brillouin frequency ( $\text{T}^{-1}$ )

$\Delta\varepsilon$  = change in strain (dimensionless,  $\text{LL}^{-1}$ )

$\Delta T$  = change in temperature ( $\Theta$ )

$C_e$  = calibrated Brillouin frequency shift-strain coefficient of the fiber ( $\text{T}^{-1}$ )

$C_T$  = calibrated Brillouin frequency shift-temperature coefficient ( $\Theta^{-1} \text{T}^{-1}$ )

Because the shift is temperature dependent, it is also necessary to measure the Raman backscatter as in DTS to compensate for any thermal effects, and therefore a Brillouin Distributed Strain Sensing (BDSS) system will have an on-board, low-resolution DTS system as well.

Strain measurements are commonly done using fiber either buried in a trench or road pavement, or a borehole. In both cases, the strain measured in the optical fiber is a function of both the true geologic strain and the mechanical coupling of the fiber to the ground. Zhang and others (2020) demonstrated that when the cable is better mechanically

connected to the geologic media (i.e., the stiffer the backfill and less stiff the cable), then more representative measures of true strain in the medium are obtained. Furthermore, increasing the gauge length, i.e., the distance over which the strain is measured in the fiber optic cable, will improve the accuracy of the true strain measurement. This is due to mechanical coupling rather than signal intensity, as is the case in DTS Raman measurements.

BDSS has been widely used in slope stability and landslide monitoring. Schenato (2017) provides an extended review of applications. However, high-end geodetic monitoring of surface displacement outperforms fiber-optic-based methods when it comes to real surface displacement in the cm or greater range as such strains can cause fiber failure. The fiber-optic-based methods are optimal for detailed strain measurements (nm-mm range), which require stiff connections. Additionally, relatively low-cost, fiber-based extensometers have been tested, which change in response to displacement. They use the principle of energy loss due to micro- or macro bending (e.g., Kwon et al., 2006; Higuchi et al., 2007). Displacement of millimeters to a few centimeters can be measured using such designs.

The hydrogeologic applications of BDSS have been limited; however, deep reservoir monitoring and geothermal monitoring continue to benefit from this technology. Its cost is higher due to the need for coincident temperature monitoring. For measurement of the rate of strain, BDSS is now being surpassed by Rayleigh-based methods.

## 4.2 Strain and Strain Rate Measurement: Distributed Acoustic Sensing (DAS)

The use of Rayleigh-based Distributed Acoustic Sensing (DAS) has recently gained prominence in the earth sciences arena. Unlike Raman or Brillouin measuring methods, which rely upon measuring the production of inelastic scattered photons, DAS uses elastically scattered Rayleigh photons to infer the rate of length change (strain) of the optical fiber. Rayleigh scattering resulting from minor heterogeneities in the refractive index is more common than Raman or Brillouin scattering and therefore provides a much larger return signal per unit time.

In a DAS system, a laser is cycled at 10 kHz or greater, and the backscattered photons return to the detector as a function of their distance down the fiber (Daley et al., 2015, Lindsey et al., 2017). The phase shift between the photons scattered from different distances down the fiber is computed for each laser pulse. To calculate the changes in fiber length over time, or strain rate, the phase shift from one laser pulse is compared to the next laser pulse, and the change in phase shift is computed. Because the rate of strain (change in length per unit time) is approximately linear to the phase shift between these two photon trains, the change in spacing between any two scattering sites can be determined (Daley et

al., 2015). As an example, if there is no fiber strain between time 1 and time 2, there will be no change in the phase shift for these two pulses. However, if a section of the fiber changes length between time 1 and time 2, then there will be a difference in phase shift observed for photons returning from this part of the fiber. For the typical laser repetition rate, the change in spacing or strain rate can be determined at frequencies well into the audible range (10 kHz) and as low as 0.1 Hz and lower (Becker et al., 2017). Typical DAS instruments today can resolve phase shifts over lengths of fiber no shorter than  $\sim 10$  m, and this measurement support scale is typically termed the instrument's *gauge length* or minimum resolvable fiber length for which a strain rate can be recovered.

DAS has been widely used in acoustic monitoring due to its very wide frequency sensitivity. In seismology, DAS is now widely used in the frequency range of earthquakes (1-10 Hz), hydrofracking, and in active seismic refraction and reflection ( $> 20$  Hz). Lindsey and others (2019) used an undersea telecommunications cable to capture both high-frequency seismic events from previously unknown features but also much lower-frequency waves, tides and storm-driven sediment transport. Li and others (2021) provide greater details of DAS application across geophysical topics.

Because DAS measures the rate of change of length between two points on the fiber, the applied stress must induce a longitudinal change in length to be measured. This makes DAS quite applicable to measuring vertical strain in boreholes driven by groundwater pumping and subsidence. In their 2017 paper, Becker and others developed an oscillatory groundwater pumping system deployed in fractured granite to test the low frequency response of DAS fibers to pumping-induced strain. Induced stress at  $\sim 0.01$  to 0.001 Hz frequencies produced only several centimeters of head change in the aquifer; however, vertical strain of up to 0.1 nm/m or 0.1 nanostrain could be recorded. Figure 11 documents the small head changes in the borehole and the resulting vertical strain recorded on the fiber in the pumping well.

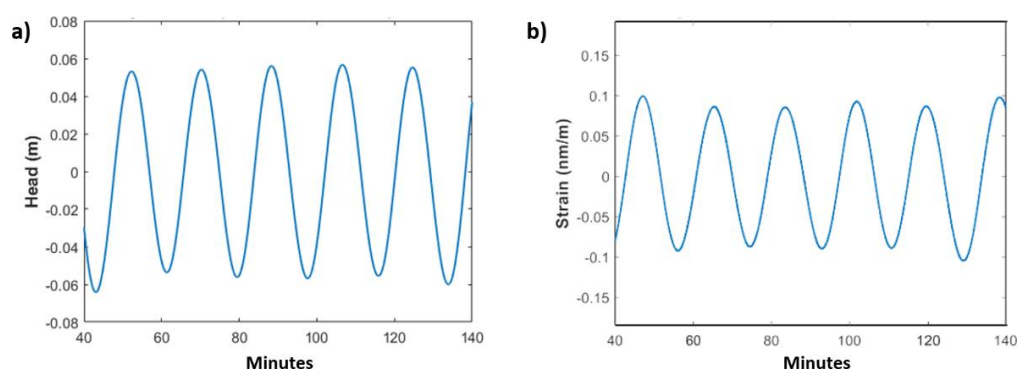


**Figure 11** - Small head changes in the borehole and the resulting vertical strain recorded on the fiber in the pumping well: a) filtered head response measured in the stressed fracture induced by pumping; and, b) observed filtered DAS strain response at the same fracture. The strain is coincident in time with the pumping and shows the dilation and contraction of the fracture in response to fluid pressure changes (Becker et al., 2017).

While this work required a modulated period driving signal (pumping) to infer the small rates of strain, many hydrogeologic stresses (earth tides, daily and seasonal groundwater pumping, flood irrigation) can be considered or designed to be quasi-periodic. Using these natural and induced stresses to infer geomechanically and hydraulic characteristics of aquifers represents a unique opportunity to obtain these characteristics at a large scale but with high spatial resolution.

Tribaldos and others (2021) successfully demonstrated that DAS could be used to monitor aquifer storage changes over large regions. Using ambient seismic noise (from automobiles and train passages) as the input energy source, the authors monitored temporal changes in seismic velocities over a 23-km long unused (“dark”) telecommunications fiber in the vicinity of the Sacramento River in central California, USA. Seismic velocity changes were observed near the river during river stage changes of ~1.5 m, as well as during periods of recharge from precipitation. The changes in seismic velocity were attributed to changes in pore pressures due to stage change or precipitation loading in the upper 10-30 meters of the aquifer. Figure 12 demonstrates the strong correlation between river stage (taken as a proxy for local groundwater levels) and the seismic velocities in the sediments adjacent to the river. Unlike point measurements, such as piezometers that provide only limited views of the aquifer response, the use of dark fiber DAS provides estimates of aquifer storage change at high spatial resolution and across very large areas. The use of DAS for large-scale aquifer monitoring in urban/suburban environments appears very promising, as buried, and unused (dark) fiber is common in urban environments. Ambient seismic noise is also ubiquitous in urban areas, and many metropolitan regions rely upon local aquifers for an important portion of their drinking water supply. These approaches may also be appropriate for more rural areas where groundwater is extensively used for irrigation, as many rural areas are transected by rail and road networks (for ambient noise) and buried telecommunication fiber commonly shares rights of way with such infrastructure.

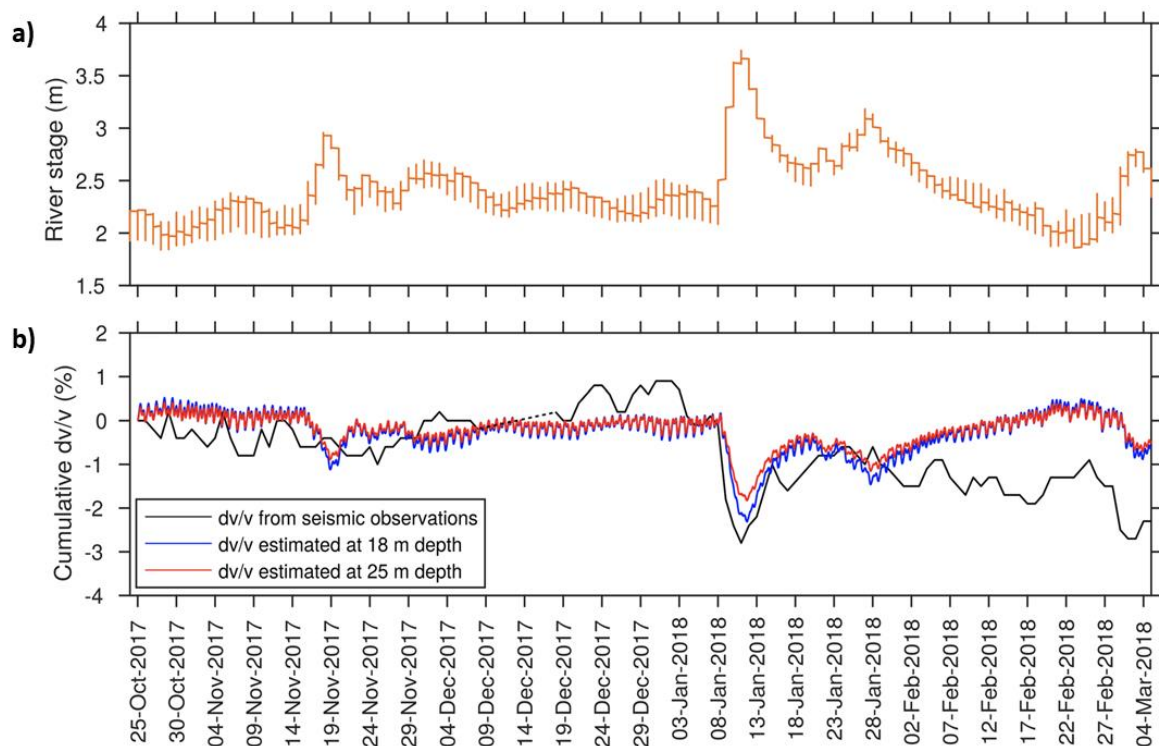


**Figure 12** - Relationship between a) Sacramento River stage; and, b) local seismic velocity changes at depth estimated from DAS inversion. Rapid rises (due to flooding) correspond to a decrease in seismic velocity as pore pressures increase, while gradual river stage decline (as seen in February 2018) corresponds to aquifer compression and an increase in seismic velocity. From Tribaldos and others (2021) with permission.

Other applications of DAS include monitoring the stability of flood embankments, in particular for slope-stability pore-pressure inference and detection of backward piping erosion (Aguilar-López et al., 2019). For the slope-stability pore-pressure application, the main physical hypothesis proposed was that the variable soil moisture content of the embankment will have a direct effect on the acoustic properties of the nearby soil matrix in contact with the cable. By deploying one single cable in multiple rows (Figure 13) over the embankment, different signals could be captured at different elevations over the embankment which could later be related to the spatially distributed moisture content.

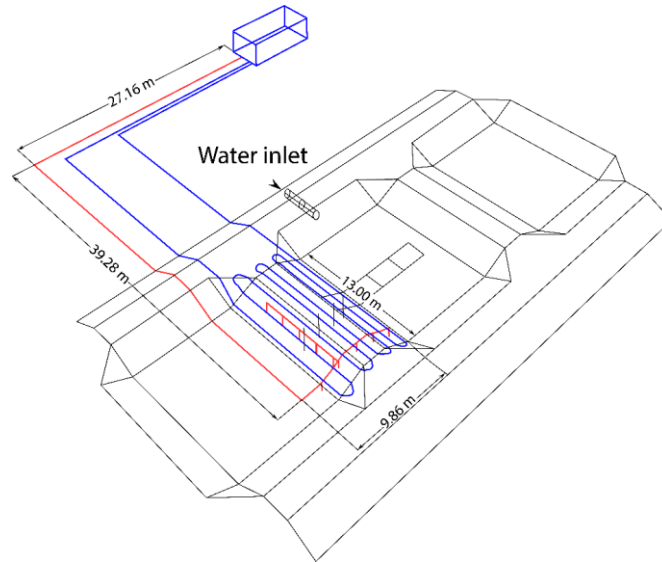


**Figure 13** - Oblique and plan view of the geometry of buried fibers (denoted by red and blue lines) within the embankment. Modified from Aguilar-López and others (2019).

The embankment was tested by using three different acoustic energy sources: 1) environment natural vibrations (passive), 2) a sledgehammer (active), and 3) a controlled seismic source with sweeps between 5 Hz and 500 Hz. In the meantime, the embankment’s inner seepage phreatic line was varied over one day. Three-minute-long measurements were taken every half hour at a frequency of 2 kHz. For validation of the measurements, 42 traditional seismic monitoring geophones and five monitoring wells were also installed as validation for the acoustics and seepage-line elevation estimated from the DAS measurements. The results show that total specific storage inside the embankment and surface wave speed are correlated on average as shown in Figure 14.

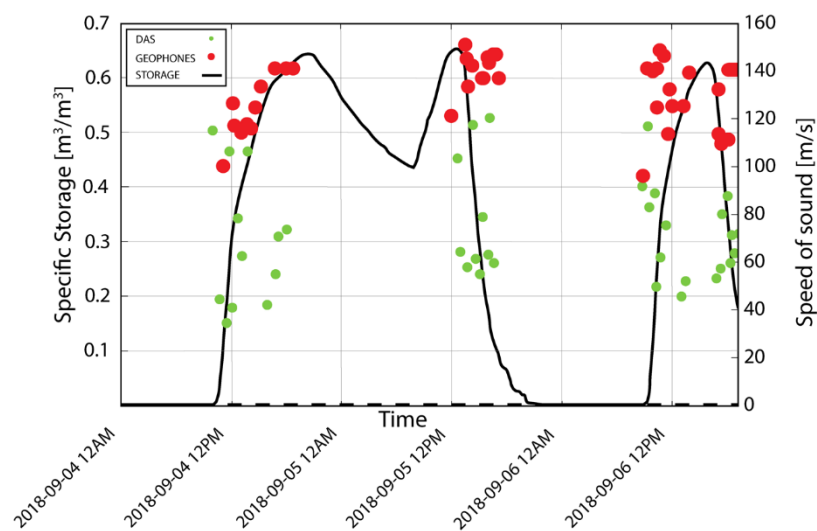


**Figure 14** - Correlation between observed seismic velocity (S-wave) and estimated embankment storage. From Aguilar-López and others (2019).

## 5 Conclusion: The Future Looks Optically Bright!

In closing, the earth sciences have been part of an instrument and computing revolution during the last two decades, often benefiting from advances in other disciplines. Fiber-based hydrogeophysical sensing has moved far beyond single point sensors and now provides truly distributed or high spatial-resolution measurements of temperature, strain, and strain rate. As our remote-sensing colleagues have been able to do for years with high spatial-resolution imagery, now hydrogeologists can resolve thermal and stress-related features at very small spatial scales in the subsurface and relatively high temporal frequency. As in all science, the closer and faster you look, the more you understand the basic physics of processes!

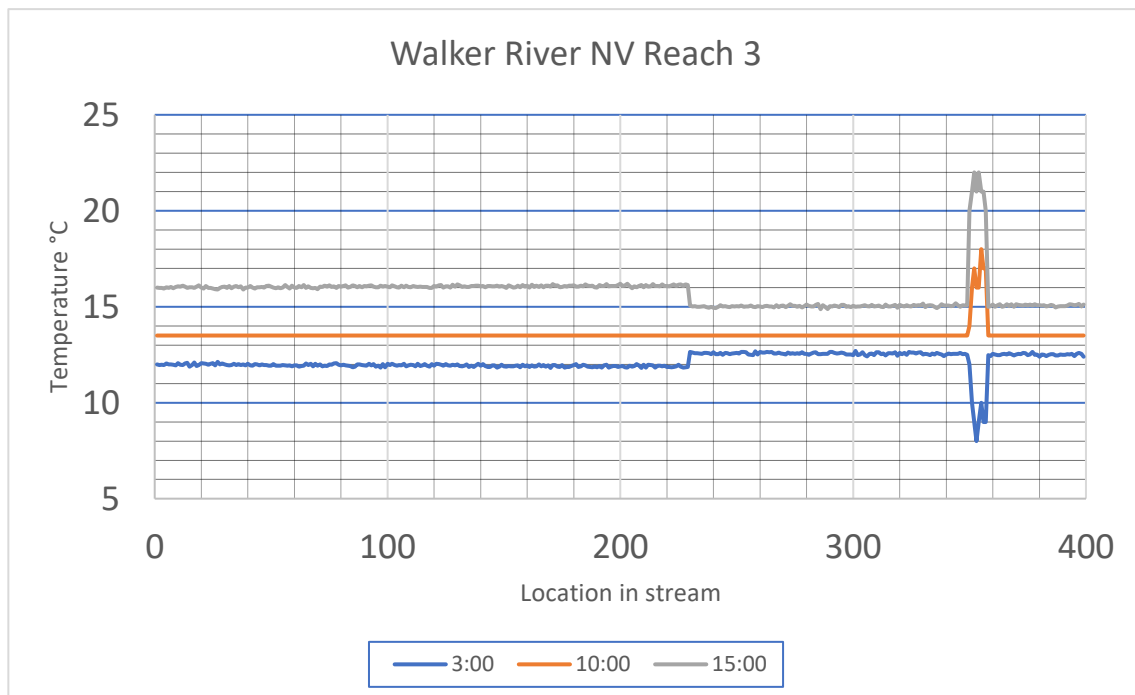
Fiber-based distributed hydrogeophysical sensing has only taken the “low-hanging” fruit to date. Buried optical fiber is ubiquitous across the built environment. Exploiting this unused telecommunication fiber could lead to a low-cost yet high-resolution continuous-monitoring network for infiltration, heat flow and strain. Just as cell-phone signals can be used to infer precipitation rates (Overeem et al., 2011; Overeem et al., 2013), existing infrastructure and tools from other industries should be explored for hydrogeophysical monitoring. The explosion in fiber-based acoustic sensing is just beginning as of this writing, with the seismology community fully embracing this new tool. Hydrogeologists and hydrogeophysicists will be needed to help these other communities understand the role of hydrology in their signals, and we too can learn from the approaches employed by others.

## 6 Exercises

### Exercise 1

The figure below shows stream temperatures measured at three different times of day (3:00, 10:00 and 15:00 hours) by an optical fiber placed at the bottom of the Walker River in western Nevada, USA, during low flow. The flow in the stream at the upstream end (0.0 meters) was measured as  $0.4 \text{ m}^3/\text{s}$  ( $\sim 14.1 \text{ ft}^3/\text{s}$ ). Using this information:

- Estimate the location of a groundwater inflow.
- Estimate the temperature of the underlying groundwater using the approach of Selker and others (2006).
- Calculate the volumetric flux (in  $\text{m}^3/\text{sec}$ ) of groundwater entering the stream at 3:00 and 15:00 hours.
- Assuming the DTS can resolve differences in temperature in space accurately to  $0.1 \text{ }^\circ\text{C}$ , what is the minimum rate of groundwater inflow that could be observed in this river given that the flow in a river is: a)  $1 \text{ m}^3/\text{s}$ ; and, b)  $10 \text{ m}^3/\text{s}$ , the stream temperature is  $15 \text{ }^\circ\text{C}$  and the groundwater differs from the stream temperature by  $5 \text{ }^\circ\text{C}$ .



Temperatures at different times of day at Walker River, Nevada, USA.

[Click for solution to Exercise 1](#) ↴

## Exercise 2

A DTS cable was installed in Martis Creek outside of Truckee California, USA, to monitor the inflow of groundwater (Avery et al., 2018). The cable ran upstream (left in the figure below) and then looped back downstream. Two well-mixed calibration baths were located at positions A and B, as shown. A long coil of cable was left in the stream at the bottom end (to the right in the figure) and a temperature sensor was placed on this coil of cable to serve as a third calibration point. Temperatures and cable positions of temperature sensors are given in the table below the figure.



DTS cable installed in Martis Creek, California, USA.

Temperatures and cable positions of temperature sensors.

Time	Bath "A" °C (9.68 to 25.92 m)	Bath "B" °C (30.99 to 55.34 m)	Downstream Cable °C (9.68 to 25.92 m)
15:10:04	19.17	-0.17	14.637
4:28:04	20.89	-0.17	16.572

The cable is duplexed and was interrogated using a single-mode operation. The data for this exercise are provided in a spreadsheet that can be downloaded by visiting the web page for this book at [gw-project.org/books/distributed-fiber-optic-hydrogeophysics/](http://gw-project.org/books/distributed-fiber-optic-hydrogeophysics/) and clicking the "Download" button.

- a) Estimate the coefficients  $\gamma$ ,  $\Delta\alpha$  and  $C$  for each DTS trace using the attached spreadsheet following the method of Hausner and others (2011) as described by Equation 2. The first trace has been calculated to provide an example and the temperature units have a conversion from Celsius to Kelvin. After the proper steps are taken to evaluate the second trace in the spreadsheet the answer will appear in cells L23-L25 in worksheet DTS RAW. It is useful to work in the the

spreadsheet striving to obtain the following values and if they are not readily attained, the solution to this exercise describes the steps needed to reach these values: Time = 4:28 hours,  $\gamma = 484.28$  °K,  $C = 1.29$  dimensionless,  $\Delta\alpha = 8.866 \times 10^{-5} \text{ m}^{-1}$ .

- b) Recalculate the DTS temperatures using the calibrated coefficients and discuss how the temperatures changed.
- c) The calibration spreadsheet uses the spatial average Stokes and anti-Stokes values from all points on the cable within each calibration bath. It is possible to estimate the DTS temperature resolution by calculating the Root Mean Squared Error (RMSE) of the DTS calibrated temperatures within each of the calibration baths. Assuming the DTS cable was uniformly at the temperature of the calibration bath, estimate the RMSE of all cable temperatures within each bath. How does the RMSE change with distance along the cable? And why?

[Click for solution to Exercise 2](#) ↴

### Exercise 3

Using data from Figure 12 of Section 4.2, develop a regression equation for the observed normalized change in seismic velocity ( $dv/V$  as a percent) and the change in aquifer storage.

[Click for solution to Exercise 3](#) ↴

## 7 References

- Abesser, C., F. Ciocca, J. Findlay, D. Hannah, P. Blaen, A. Chalari, M. Mondanos, and S. Krause, 2020, A distributed heat pulse sensor network for thermo-hydraulic monitoring of the soil subsurface. *Quarterly Journal of Engineering and Hydrogeology*, volume 53, issue 3, page 352-365, <http://doi.org/10.1144/qjegh2018-147>.
- Avery, E., R. Bibby, A. Visser, B. Esser, and J. Moran, 2018, Quantification of groundwater discharge in a subalpine stream using Radon-222. *Water*, volume 10, issue 2, page 100, <https://doi.org/10.3390/w10020100>.
- Aguilar-López, J.P., T.A. Bogaard, A.G. Ruiz, M.G. Herràez, and G.G. Drijkoningen, 2019, Fiber optic distributed acoustic sensing for levee monitoring. *European Geosciences Union General Assembly*, Vienna, Austria, <http://resolver.tudelft.nl/uuid:c3816121-4354-4046-a15b-37cab3d3363f>, Accessed on May 27, 2022.
- Bakker, M., R. Caljé, F. Schaars, K.J. van der Made, and S. Haas, 2015, An active heat tracer experiment to determine groundwater velocities using fiber optic cables installed with direct push equipment. *Water Resources Research*, volume 51, issue 4, pages 2760-2772, <https://doi.org/10.1002/2014WR016632>.
- Bakx, W., P.J. Doornenbal, R.J. van Weesep, V.F. Bense, G.H.P.O. Essink, and M.F.P. Bierkens, 2019, Determining the relation between groundwater flow velocities and measured temperature differences using active heating-distributed temperature sensing. *Water*, volume 11, issue 8, page 1619, <https://doi.org/10.3390/w11081619>.
- Banks, E., M. Shannafield, and P. Cook, 2014, Induced temperature gradients to examine groundwater flowpaths in open boreholes. *Groundwater*, volume 52, issue 6, pages 943-951, <https://doi.org/10.1111/gwat.12157>.
- Becker, M.W., C. Ciervo, M. Cole, T. Coleman, and M. Mondanos, 2017, Fracture hydromechanical response measured by fiber optic distributed acoustic sensing at milli-Hertz frequencies. *Geophysical Research Letters*, volume 44, issue 14, pages 7295-7302, <https://doi.org/10.1002/2017GL073931>.
- Bencala, K.E., 2000, Hyporheic zone hydrological processes. *Hydrological Processes*, volume 14, issue 15, pages 2797-2798, [https://doi.org/10.1002/1099-1085\(20001030\)14:15<2797::AID-HYP402>3.0.CO;2-6](https://doi.org/10.1002/1099-1085(20001030)14:15<2797::AID-HYP402>3.0.CO;2-6).
- Benítez-Buelga, J., C. Sayde, L. Rodríguez-Sinobas, and J.S. Selker, 2014, Heated fiber optic distributed temperature sensing: a dual-probe heat-pulse approach. *Vadose Zone Journal*, volume 13, issue 11, pages 1-10, <https://doi.org/10.2136/vzj2014.02.0014>.

- Bense, V.F., T. Read, O. Bour, T. Le Borgne, T. Coleman, S. Krause, A. Chalari, M. Mondanos, F. Ciocca, and J.S. Selker, 2016, Distributed temperature sensing as a downhole tool in hydrogeology. *Water Resources Research*, volume 52, issue 12, pages 9259-9273, <https://doi.org/10.1002/2016WR018869>.
- Briggs, M.A., L.K. Lautz, and J.M. McKenzie, 2012, A comparison of fibre-optic distributed temperature sensing to traditional methods of evaluating groundwater inflow to streams. *Hydrologic Processes*, volume 26, issue 9, pages 1277-1290, <https://doi.org/10.1002/hyp.8200>.
- Blume, T., S. Krause, K. Meinikmann, and J. Lewandowski, 2013, Upscaling lacustrine groundwater discharge rates by fiber-optic distributed temperature sensing. *Water Resources Research*, volume 49, issue 12, pages 7929-7944, <https://doi.org/10.1002/2012WR013215>.
- Bersan, S., A.R. Koelewijn, and P. Simonini, 2017, Effectiveness of distributed temperature measurements for early detection of piping in river embankments. *Hydrology Earth System Sciences*, volume 22, pages 1491-1508, <https://doi.org/10.5194/hess-22-1491-2018>.
- Ciocca, F., I. Lunati, N. Van de Giesen, and M.B. Parlange, 2012, Heated optical fiber for distributed soil-moisture measurements: A lysimeter experiment. *Vadose Zone Journal*, volume 11, issue 4, <https://doi.org/10.2136/vzj2011.0199>.
- Coleman, T.I., B.L. Parker, C.H. Maldaner, and M.J. Mondanos, 2015, Groundwater flow characterization in a fractured bedrock aquifer using active DTS tests in sealed boreholes. *Journal of Hydrology*, volume 528, pages 449-462, <https://doi.org/10.1016/j.jhydrol.2015.06.061>.
- Constantz, J., 1998, Interaction between stream temperature, streamflow, and groundwater exchanges in alpine streams. *Water Resources Research*, volume 34, issue 7, pages 1609-1615, <https://doi.org/10.1029/98WR00998>.
- Daley, T.M., D.E. Miller, K. Dodds, P. Cook, and B.M. Freifeld, 2015, Field testing of modular borehole monitoring with simultaneous distributed acoustic sensing and geophone vertical seismic profiles at Citronelle, Alabama. *Geophysical Prospecting*, volume 64, issue 5, pages 1318-1334, <https://doi.org/10.1111/1365-2478.12324>.
- des Tombe, B.F., M. Bakker, F. Smits, F. Schaars, and K.-J. van der Made, 2019, Estimation of the variation in specific discharge over large depth using distributed temperature sensing (DTS) measurements of the heat pulse response. *Water Resources Research*, volume 55, issue 1, pages 811-826, <https://doi.org/10.1029/2018WR024171>.
- des Tombe, B.F. and B. Schilperoort, 2020a, DTS calibration Python package for calibrating distributed temperature sensing measurements. <https://zenodo.org/record/3876407-.YRCkoNNKi3I>, Accessed on May 27, 2022.

- des Tombe, B., B. Schilperoort, and M. Bakker, 2020b, Estimation of temperature and associated uncertainty from fiber-optic Raman-spectrum distributed temperature sensing. *Sensors*, volume 20, issue 8, page 2235, <https://doi.org/10.3390/s20082235>.
- Dong, J., S.C. Steele-Dunne, T.E. Ochsner, C.E. Hatch, C. Sayde, J. Selker, S. Tyler, M.H. Cosh, and N. Van de Giesen, 2016, Mapping high-resolution soil moisture and properties using distributed temperature sensing data and an adaptive particle batch smoother. *Water Resources Research*, volume 52, issue 10, pages 7690-7710, <https://doi.org/10.1002/2016WR019031>.
- Dong, J., R. Agliata, S. Steele-Dunne, O. Hoes, T. Bogaard, R. Greco, and N. Van de Giesen, 2017, The impacts of heating strategy on soil moisture estimation using actively heated fiber optics. *Sensors*, volume 17, issue 9, page 2102, <https://doi.org/10.3390/s17092102>.
- Farahani, M. and T. Gogolla, 1999, Spontaneous Raman scattering in optical fibers with modulate probe light for distributed temperature Raman remote. *Journal of Lightwave Technology*, volume 17, issue 8, pages 1379-1391, [doi: 10.1109/50.779159](https://doi.org/10.1109/50.779159).
- Freifeld, B.M., S. Finsterle, T.C. Onstott, P. Toole, and L.M. Pratt, 2008, Ground surface temperature reconstructions: using in situ estimates for thermal conductivity acquired with a fiber-optic distributed thermal perturbation sensor. *Geophysical Research Letters*, volume 35, issue 14, <https://doi.org/10.1029/2008GL034762>.
- Ghafoori, Y., A. Vidmar, J. Říha, and A. Kryžanowski, 2020, A review of measurement calibration and interpretation for seepage monitoring by optical fiber distributed temperature. *Sensors*, volume 20, issue 19, page 5696, <https://doi.org/10.3390/s20195696>.
- Gregory, C.T., 2009, Temperature and infiltration characterization of a constructed wetland for wastewater treatment. Master of Science Thesis, Department of Biological and Ecological Engineering, Oregon State University, 97 pages, <http://hdl.handle.net/1957/13780>, Accessed on 27 May, 2022.
- Hausner, M.B., S. Suárez, K.E. Glander, N. Van de Giesen, J.S. Selker, and S. Tyler, 2011, Calibrating single-ended fiber-optic Raman spectra distributed temperature sensing data. *Sensors*, volume 11, issue 11, pages 10859-10879, <https://doi.org/10.3390/s111110859>.
- Hausner, M.B., L. Kryder, J. Klenke, R. Reinke, and S.W. Tyler, 2016, Interpreting variations in groundwater flows from repeated distributed thermal perturbation tests. *Groundwater*, volume 54, issue 4, pages 559-568, <https://doi.org/10.1111/gwat.12393>.
- Hawkins, A.J., D.B. Fox, M.W. Becker, and J.W. Tester, 2017, Measurement and simulation of heat exchange in fractured bedrock using inert and thermally degrading tracers.

- Water Resources Research, volume 53, issue 2, pages 1210-1230,  
<https://doi.org/10.1002/2016WR019617>.
- He, H., M.F. Dyck, R. Horton, T. Ren, K.L. Bristow, J. Lv, and B. Si, 2018, Development and application of the heat pulse method for soil physical measurements. *Reviews of Geophysics*, volume 56, issue 4, pages 567-620,  
<https://doi.org/10.1029/2017RG000584>.
- Henderson, R.D., F.D. Day-Lewis, and C.F. Harvey, 2009, Investigation of aquifer-estuary interaction using wavelet analysis of fiber-optic temperature data. *Geophysical Research Letters*, volume 36, issue 6, <https://doi.org/10.1029/2008GL036926>.
- Higuchi, K., K. Fujisawa, K. Asai, A. Pasuto, and G. Marcato, 2007, Application of new landslide monitoring technique using optical fiber sensor at Takisaka Landslide, Japan. *Proceedings of the First North American Landslide Conference*, Vail, Colorado, USA, pages 1074-1083,  
<https://www.pwri.go.jp/team/landslide/outcome/102.pdf>, Accessed on 27 May, 2022.
- Hill, K.O. and G. Meltz, 1997, Fiber Bragg grating technology: fundamentals and overview. *Journal of Lightwave Technology*, volume 15, issue 8, pages 1263-1276,  
<https://doi.org/10.1109/50.618320>.
- Johansson, S., 1997, Seepage monitoring in embankment dams. Doctor of Philosophy thesis, Superseded Departments, Civil and Environmental Engineering, Royal Institute of Technology, Stockholm, Sweden,  
<http://urn.kb.se/resolve?urn=urn:nbn:se:kth:diva-2477>, Accessed on May 27, 2022.
- Johansson, S. and P. Sjö Dahl, 2004, Downstream seepage detection using temperature measurements and visual inspection—Monitoring experiences from Røsvatn field test dam. *Seminar on Stability and Breaching of Embankment Dams*, Oslo, Norway, 21–22 October 2004, 20 pages,  
[https://www.sensonet.co.uk/wp-content/uploads/2016/05/Oslo\\_2004-Downstream-Seepage-Detection-using-Temperature-Me.pdf](https://www.sensonet.co.uk/wp-content/uploads/2016/05/Oslo_2004-Downstream-Seepage-Detection-using-Temperature-Me.pdf), Accessed on May 27, 2022.
- Johansson, S. and P. Sjö Dahl, 2007, Seepage measurements and internal erosion detection using the passive temperature method *in* *Assessment of the Risk of Internal Erosion of Water Retaining Structures: Dams, Dykes and Levees*, Technische Universität München, Munich, Germany, pages 186-192, ISBN 978-3-940476-04-3.
- Klepikova, M., C. Roques, S. Loew, and J.S. Selker, 2018, Improved characterization of groundwater flow in heterogeneous aquifers using granular polyacrylamide (PAM) gel as temporary grout. *Water Resources Research*, volume 54, issue 2, pages 1410-1419, <https://doi.org/10.1002/2017WR022259>.

- Kishida, K., Y. Yamauchi, and A. Guzik, 2014, Study of optical fibers strain-temperature sensitivities using hybrid Brillouin-Rayleigh system. *Photonic Sensors*, volume 4, issue 1, pages 1-11, <https://doi.org/10.1007/s13320-013-0136-1>.
- Kwon, I.B., C.Y. Kim, D.C. Seo, and H.C. Hwang, 2006, Multiplexed fiber optic OTDR sensors for monitoring of soil sliding. *Proceedings of the XVIII IMEKO World Congress, Rio de Janeiro, Brazil, 17-22 September 2006*, <https://www.imeko.org/publications/wc-2006/PWC-2006-TC20-002u.pdf>, Accessed on May 27, 2022.
- Leaf, A.T., D.J. Hart, and J.M. Bahr, 2012, Active thermal tracer tests for improved hydrostratigraphic characterization. *Groundwater*, volume 50, issue 5, pages 726-735, <https://doi.org/10.1111/j.1745-6584.2012.00913.x>.
- Li, Y., M. Karrenbach, and J. Ajo-Franklin, editors, 2021, *Distributed acoustic sensing in geophysics: methods and applications*. American Geophysical Union Monograph, ISBN: 978-1-119-52177-8, 320 pages.
- Lindsey, N.J., E.R. Martin, D.S. Dreger, B. Freifeld, S. Cole, S.R. James, and J.B. Ajo-Franklin, 2017, Fiber-optic network observations of earthquake wavefields. *Geophysical Research Letters*, volume 44, issue 23, pages 11,792-11,799, <https://doi.org/10.1002/2017GL075722>.
- Lindsey, N.J., T.C. Dawe, and J.B. Ajo-Franklin, 2019, Illuminating seafloor faults and ocean dynamics with dark fiber distributed acoustic sensing. *Science*, volume 366, issue 6469, pages 1103-1107, <https://doi.org/10.1126/science.aay5881>.
- Maldaner, C.H., J.D. Munn, T.I. Coleman, J.W. Molson, and B.L. Parker, 2019, Groundwater flow quantification in fractured rock boreholes using active distributed temperature sensing under natural gradient conditions. *Water Resources Research*, volume 55, issue 4, pages 3285-3306, <https://doi.org/10.1029/2018WR024319>.
- McDaniel, A., D. Fratta, J.M. Tinjum, and D. Hart, 2017, Long-term district-scale geothermal exchange borefield monitoring with fiber optic distributed temperature sensing. *Geothermics*, volume 72, pages 193-204, <https://doi.org/10.1016/j.geothermics.2017.11.008>.
- Medina, R., C. Pham, M. Plumlee, A. Hutchinson, M. Becker, and P. Connell, 2020, Distributed temperature sensing to measure infiltration rates across a groundwater recharge basin. *Groundwater*, volume 58, issue 6, pages 913-923, <https://doi.org/10.1111/gwat.13007>.
- Nyquist, H., 1928, Certain topics in telegraph transmission theory. *Winter Convention of the American Institute of Electrical Engineers, New York, February 13-17*, pages 617-644, [https://www.eit.lth.se/fileadmin/eit/courses/eit085f/Nyquist\\_Certain\\_Topics\\_in\\_Telegraph\\_Transmission\\_Theory\\_AIEE\\_1928.pdf](https://www.eit.lth.se/fileadmin/eit/courses/eit085f/Nyquist_Certain_Topics_in_Telegraph_Transmission_Theory_AIEE_1928.pdf), Accessed on May 27, 2022.

- Overeem, A., H. Leijnse, and R. Uijlenhoet, 2011, Measuring urban rainfall using microwave links from commercial cellular communication networks. *Water Resources Research*, volume 47, issue 12, <https://doi.org/10.1029/2010WR010350>.
- Overeem, A., H. Leijnse, and R. Uijlenhoet, 2013, Country-wide rainfall maps from cellular communication networks. *Proceedings of the National Academy of Sciences of United States of America*, volume 110, issue 8, 2741-2745, <https://doi.org/10.1073/pnas.1217961110>.
- Perzmaier, S., M. Aufleger, and M. Conrad, 2004, Distributed fiber optic temperature measurements in hydraulic engineering: Prospects of the heat-up method. *Proceedings of a Workshop on Dam Safety Problems and Solutions, 72nd Annual Meeting, Workshop on Dam Safety Problems and Solutions-Sharing Experience, Seoul, South Korea*, page 31.
- Perzmaier, S., M. Aufleger, and J. Dornstädter, 2007, Detection of internal erosion by means of the active temperature method *in* *Assessment of the Risk of Internal Erosion of Water Retaining Structures: Dams, Dykes and Levees*, Technische Universität München, Munich, Germany, ISBN 978-3-940476-04-3.
- Read, T., O. Bour, J.S. Selker, V.F. Bense, T.L. Borgne, R. Hochreutener, and N. Lavenant, 2014, Active-distributed temperature sensing to continuously quantify vertical flow in boreholes. *Water Resources Research*, volume 50, issue 5, pages 3706-3713, <https://doi.org/10.1002/2014WR015273>.
- Read, T., V.F. Bense, R. Hochreutener, O. Bour, T. Le Borgne, N. Lavenant, and J.S. Selker, 2015, Thermal-plume fibre optic tracking (T-POT) test for flow velocity measurement in groundwater boreholes. *Geoscientific Instrumentation, Methods and Data Systems*, volume 4, issue 2, pages 197-202, <https://doi.org/10.5194/gi-4-197-2015>.
- Rose, L., S. Krause, and N.J. Cassidy, 2013, Capabilities and limitations of tracing spatial temperature patterns by fiber-optic distributed temperature sensing. *Water Resources Research*, volume 49, issue 3, pages 1741-1745, <https://doi.org/10.1002/wrcr.20144>.
- Sayde, C., J.B. Buelga, L. Rodriguez-Sinobas, L.E. Khoury, M. English, N. Van de Giesen, and J.S. Selker, 2014, Mapping variability of soil water content and flux across 1-1000 m scales using the Actively Heated Fiber Optic method. *Water Resources Research*, volume 50, issue 9, pages 7302-7317, <https://doi.org/10.1002/2013WR014983>.
- Sayde, C., C. Gregory, M. Gil-Rodriguez, N. Tuffillaro, S. Tyler, N. Van de Giesen, M. English, R. Cuenca, and J.S. Selker, 2010, Feasibility of soil moisture monitoring with heated fiber optics. *Water Resources Research*, volume 46, issue 6, <https://doi.org/10.1029/2009WR007846>.

- Schenato, L., 2017, A review of distributed fibre optic sensors for geo-hydrological applications. *Applied Sciences*, volume 7, issue 9, page 896, <https://doi.org/10.3390/app7090896>.
- Selker, J., N. Van de Giesen, M. Westhoff, W. Luxemburg, and M.B. Parlange, 2006a, Fiber optics opens window on stream dynamics. *Geophysical Research Letters*, volume 33, issue 24, <https://doi.org/10.1029/2006GL027979>.
- Selker, J.S., L. Thévenaz, H. Huwald, A. Mallet, W. Luxemburg, N. Van de Geisen, M. Stejskal, J. Zeman, M. Westoff, and M.B. Parlange, 2006b, Distributed fiber-optic temperature sensing for hydrologic systems. *Water Resources Research*, volume 42, issue 12, <https://doi.org/10.1029/2006WR005326>.
- Selker, J.S., S. Tyler, and N. Van de Giesen, 2014, Comment on “Capabilities and limitations of tracing spatial temperature patterns by fiber-optic distributed temperature sensing” by L. Rose, S. Krause, and N.J. Cassidy. *Water Resources Research*, volume 50, issue 6, pages 5372-5374, <https://doi.org/10.1002/2013WR014979>.
- Selker, F. and J.S. Selker, 2018, Investigating water movement within and near wells using active point heating and fiber optic distributed temperature sensing. *Sensors*, volume 18, issue 4, page 1023, <https://doi.org/10.3390/s18041023>.
- Shanafield, M., E.W. Banks, J.W. Arkwright, and M.B. Hausner, 2018, Fiber-optic sensing for environmental applications: Where we have come from and what is possible. *Water Resources Research*, volume 54, issue 11, page 8552-8557, <https://doi.org/10.1029/2018WR022768>.
- Simon, N., O. Bour, N. Lavenant, G. Porel, B. Nauleau, B. Pouladi, and L. Longuevergne, 2020, A comparison of different methods to estimate the effective spatial resolution of FO-DTS measurements achieved during sandbox experiments. *Sensors*, volume 20, issue 2, <https://doi.org/10.3390/s20020570>.
- Sourbeer, J. and S. Loheide, 2015, Obstacles to long-term soil moisture monitoring with heated distributed temperature sensing. *Hydrological Processes*, volume 30, issue 7, pages 1017-1035, <https://doi.org/10.1002/hyp.10615>.
- Steele-Dunne, S.C., M.M. Rutten, D.M. Krzeminska, M. Hausner, S.W. Tyler, J. Selker, T.A. Bogaard, and N.C. Van de Giesen, 2010, Feasibility of soil moisture estimation using passive distributed temperature sensing. *Water Resources Research*, volume 46, issue 3, <https://doi.org/10.1029/2009WR008272>.
- Tribaldos, V.R. and J.B. Ajo-Franklin, 2021, Aquifer monitoring using ambient seismic noise recorded with distributed acoustic sensing (DAS) deployed on dark fiber. *Journal of Geophysical Research: Solid Earth*, volume 126, issue 4, <https://doi.org/10.1029/2020JB021004>.

- Tyler, S.W., S. Burak, J. McNamara, A. Lamontagne, J. Selker, and J. Dozier, 2008, Spatially distributed temperatures at the base of two mountain snowpacks measured with fiber-optic sensors. *Journal of Glaciology*, volume 54, issue 187, pages 673-679, <https://doi.org/10.3189/002214308786570827>.
- Tyler, S.W., J.S. Selker, M.B. Hausner, C.E. Hatch, T. Torgersen, C.E. Thodal, and S.G. Schladow, 2009, Environmental temperature sensing using Raman spectra DTS fiber optic methods. *Water Resources Research*, volume 45, issue 4, <https://doi.org/10.1029/2008WR007052>.
- Uijlenhoet, R., A. Overeem, and H. Leijnse, 2018, Opportunistic remote sensing of rainfall using microwave links from cellular communication networks. *Wiley Interdisciplinary Reviews*, volume 5, issue 4, <https://doi.org/10.1002/wat2.1289>.
- Van de Giesen, N., S.C. Steele-Dunne, J. Jansen, O. Hoes, M.B. Hausner, S. Tyler, and J. Selker, 2012, Double-ended calibration of fiber-optic Raman spectra distributed temperature sensing data. *Sensors*, volume 12, issue 5, pages 5471-5485, <https://doi.org/10.3390/s120505471>.
- Weiss, J.D., 2012, Using fiber optics to detect moisture intrusion into a landfill cap consisting of a vegetative soil barrier. *Journal of the Air and Waste Management Association*, volume 53, issue 9, pages 1130-1148, <https://doi.org/10.1080/10473289.2003.10466268>.
- Westhoff, M.C., H.H.G. Savenije, W.M.J. Luxemburg, G.S. Stelling, N.C. Van de Giesen, J.S. Selker, L. Pfister, and S. Uhlenbrook, 2007, A distributed stream temperature model using high resolution temperature observations. *Hydrology and Earth System Sciences*, volume 11, pages 1469-1480, <https://doi.org/10.5194/hess-11-1469-2007>.
- Wu, R., V. Martin, J. McKenzie, S. Broda, B. Bussière, M. Aubertin, and B.L. Kurylyk, 2019, Laboratory-scale assessment of a capillary barrier using fibre optic distributed temperature sensing (FO-DTS). *Canadian Geotechnical Journal*, volume 57, issue 1, pages 115-126, <https://doi.org/10.1139/cgj-2018-0283>.
- Zhang, C.-C., B. Shi, H.-H. Zhu, B.-J. Wang, and G.-Q. Wei, 2020, Toward distributed fiber-optic sensing of subsurface deformation: A theoretical quantification of ground-borehole-cable interaction. *Journal of Geophysical Research: Solid Earth*, volume 125, issue 3, <https://doi.org/10.1029/2019JB018878>.

## 8 Exercise Solutions

### Solution Exercise 1

- a) At ~230 m down the fiber, the stream temperature abruptly cools during the warmest part of the day (15:00 hours) and abruptly warms during the coolest part of the day (3:00 hours). This cooling and warming carries on downstream. To cool the stream temperature in the middle of the day, cooler groundwater must be entering at ~230 m. At ~350 m down the stream, the fiber records a significant rise in “stream” temperature during the day and a significant cooling at night, but these changes are not carried downstream, and the stream returns to the temperature upstream of the excursions. In this case, the fiber is probably either out of the stream and in the air or very, very close to the stream surface, where it can warm by solar radiation. This may be an intentional placement of the cable above the water or accidental after initial installation. In either case, the excursions in temperature match the timing of air temperature and solar radiation, in contrast to inflowing groundwater which is opposite in phase from the daily warming and cooling.
- b) At 3:00 and 15:00 hours, the stream temperature changes abruptly at ~230 meters indicating a groundwater inflow. At 10:00 hours, there is no change in stream temperature at 230 meters, indicating that the groundwater and stream water are at the same temperature. In this case, from the figure, the stream temperature is ~13.5 °C, and so the groundwater temperature must also be ~13.5 °C ( $T_g = 13.5$  °C).
- c) For the 15:00-hour profile, the upstream temperature,  $T_i$ , is 16 °C while the downstream temperature  $T_o$  is 15 °C and the upstream inflow is given as  $Q_i = 0.4$  m<sup>3</sup>/sec, Assuming the groundwater temperature is 13.5 °C, from Selker and others (2006), the energy balance reduces to the following.

$$Q_i T_i + Q_g T_g = Q_o T_o = (Q_i + Q_g) T_o$$

Or

$$\frac{Q_i}{Q_g} = \frac{(T_o - T_g)}{(T_i - T_o)}$$

Or

$$Q_g = Q_i \left( \frac{T_i - T_o}{T_o - T_g} \right)$$

Substituting

$$Q_g = 0.4 \frac{\text{m}^3}{\text{s}} \frac{16^\circ\text{C} - 15^\circ\text{C}}{15^\circ\text{C} - 13.5^\circ\text{C}} = 0.4 \frac{\text{m}^3}{\text{s}} 0.67 = 0.267 \frac{\text{m}^3}{\text{s}}$$

Note that this is quite a large inflow of groundwater and would likely be visible as an increase in streamflow.

- d) If the DTS can resolve, at best, differences in temperature from one location to the next of 0.05 °C, then we can begin to estimate the smallest flux measurable under “typical” groundwater temperatures. For example, if groundwater is 5 °C different than the stream temperatures, then what is the groundwater inflow needed to lower (or raise) the stream temperature by 0.05 °C. We can express the downstream temperature  $T_o$  as the upstream temperature  $T_i$  plus the measurable difference of -0.1 °C (we use a negative difference here assuming the groundwater is colder than the stream, which is common during summer daytime hours, and we use 0.1 instead of 0.05 because we can only measure the temperature +/-0.05 so if we are 0.05 too low on the upstream and 0.05 too high on the downstream then there appears to be no inflow), then simplify the heat balance equation presented at the end of part (c) as follows.

$$Q_g = Q_i \left( \frac{T_i - T_o}{T_o - T_g} \right)$$

$$Q_g = Q_i \left( \frac{T_i - (T_i + -0.10 \text{ °C})}{T_o - T_g} \right)$$

$$Q_g = Q_i \left( \frac{0.10 \text{ °C}}{T_o - T_g} \right)$$

Or

$$\frac{Q_g}{Q_i} = \frac{0.1 \text{ °C}}{15 \text{ °C} - 5 \text{ °C}} = 0.01 \text{ or } 1.0\%$$

Thus, for streamflow  $Q_i$  of 1 m<sup>3</sup>/sec, we can resolve 0.01 m<sup>3</sup>/sec of groundwater inflow  $Q_g$  or ~10 liters/sec. For a larger river of 10 m<sup>3</sup>/sec, the best we can resolve is 0.1 m<sup>3</sup>/sec, which is a large groundwater inflow. As stream volume grows, the ability of DTS to detect small groundwater inflow decreases due to the resolution of the DTS, unlike chemical tracers that can be detected in the parts per million. DTS typically detects changes in the “parts per 100”.

[Return to Exercise 1](#) ↴

## Solution Exercise 2

- a) On the spreadsheet sheet “DTS RAW”, the temperature values of the calibration baths have been inserted for the time 4:28 hours, along with the calculated average Stokes and anti-Stokes signals from the sections of the fiber in each of the calibration baths. The “A” matrix for the calibration equation has also been populated for the 4:28 hours. Begin the process of calibration by taking the matrix inverse of A using the Excel matrix inversion function “MINVERSE”. Next, the “b” matrix has already been populated for you with the product of the bath temperatures and the ratio of the log of Stokes and anti-Stokes power from time = 4:28 hours. Finally, calculate the calibration parameters by making the matrix multiplication of  $A^{-1} * b$  using the Excel function MMULT . The resulting calibration parameter should be:

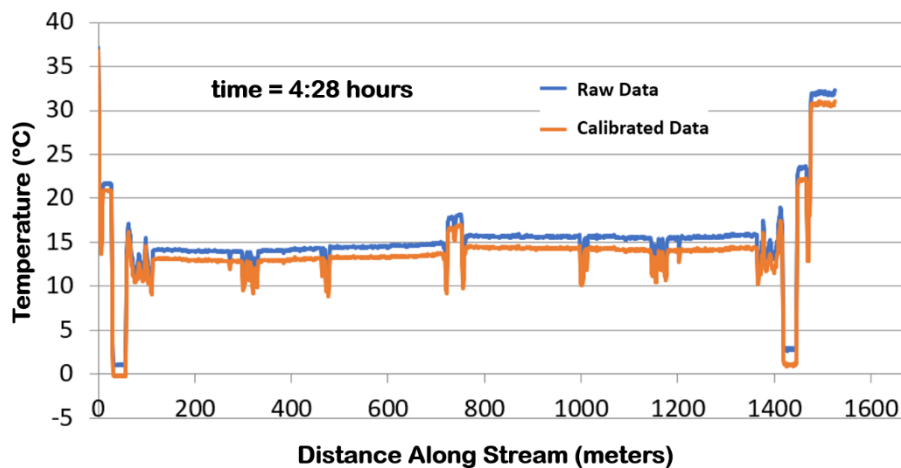
Time = 4:28 hours

$\gamma = 484.28 \text{ K}$

$C = 1.29$  (dimensionless)

$\Delta\alpha = 8.866 \times 10^{-5} \text{ m}^{-1}$

- b) Shown below are the measured stream temperatures at 4:28 (in blue) as compared to the calibrated ones using the calibration coefficients from part a and the calibration equation. To calculate the calibrated temperatures, you can copy the calibration equation over from time = 3:10 PM (column. F in DTS RAW sheet) and past into and paste into column L, being sure to adjust the cell calls to call the DTS data from 4:28 hours. Overall, the calibration reduced the stream temperatures by a relatively similar amount, suggesting that the presumed differential attenuation coefficient was close to the correct value, i.e., there was little slope change in the results as shown in the figure below.



Raw and calibrated data for 4:28 hours trace.

- c) First calculate the Root Mean Squared Error (RMSE) from each 10 m length of fiber in each of the calibration baths used in the calibration. The RMSE is calculated as shown below:

$$RMSE = \sqrt{\frac{\sum_{i=1}^n (T(z_i) - T_{bath})^2}{n}}$$

where:

$T(z_i)$  = calibrated temperature at each point on the calibration section, in this case from 9.68 m to 25.9 m for Bath 1 (including 17 measurements), from 30.99 m to 55.34 m for Bath 2 (including 25 measurements) and from 724.99 m to 736.13 m for Bath 3 (including 24 measurements)

$T_{bath}$  = assumed “true” temperature of the bath as measured by the independent temperature sensor

$n$  = number of observations (in this case 17 points for Bath 1, 25 points for bath 2 and 24 points for Bath 3)

The calculated temperatures from both traces within the two calibrations baths, and the corresponding measured bath temperatures are shown in the table below.

Data from two DTS traces within calibration baths. Calibration Bath 1 begins at 9.688 m and ends at 25.92 m. Calibration Bath 2 begins at 30.994 m and ends at 55.344 m. Calibration Bath 3 begins 724.99 m and ends at 736.13 m. Transitions between Baths are indicated by shading.

Time = 15:10			Time = 4:28		
Cable distance (m)	T <sub>calibrated</sub>	T <sub>bath</sub>	Cable distance (m)	T <sub>calibrated</sub>	T <sub>bath</sub>
9.688	19.20064958	19.17	9.688	20.84919341	20.89
10.702	19.02876606	19.17	10.702	20.86304149	20.89
11.717	19.12327031	19.17	11.717	20.85627611	20.89
12.731	19.13207407	19.17	12.731	20.9300866	20.89
13.746	19.15839026	19.17	13.746	20.92466545	20.89
14.761	19.20355003	19.17	14.761	20.9146521	20.89
15.775	19.26246247	19.17	15.775	20.91940108	20.89
16.79	19.2119609	19.17	16.79	20.85922323	20.89
17.804	19.18031936	19.17	17.804	20.90630153	20.89
18.819	19.1534668	19.17	18.819	20.89528913	20.89
19.834	19.23392457	19.17	19.834	20.96513629	20.89
20.848	19.18208139	19.17	20.848	20.87671062	20.89
21.863	19.10911496	19.17	21.863	20.84182784	20.89
22.877	19.23165354	19.17	22.877	20.94894786	20.89

23.892	19.15091432	19.17	23.892	20.81938265	20.89
24.907	19.14782634	19.17	24.907	20.8582565	20.89
25.921	19.18368123	19.17	25.921	20.90557791	20.89
30.994	0.148849032	-0.17	30.994	0.048998697	-0.17
32.009	-0.150060865	-0.17	32.009	-0.094790973	-0.17
33.023	-0.170548613	-0.17	33.023	-0.245489913	-0.17
34.038	-0.217096836	-0.17	34.038	-0.17536847	-0.17
35.053	-0.249312361	-0.17	35.053	-0.276940387	-0.17
36.067	-0.185950565	-0.17	36.067	-0.218028531	-0.17
37.082	-0.18260034	-0.17	37.082	-0.230442845	-0.17
38.096	-0.2037029	-0.17	38.096	-0.226951929	-0.17
39.111	-0.148092379	-0.17	39.111	-0.128530218	-0.17
40.126	-0.188837919	-0.17	40.126	-0.189548408	-0.17
41.14	-0.22549814	-0.17	41.14	-0.288113919	-0.17
42.155	-0.193666694	-0.17	42.155	-0.250570457	-0.17
43.169	-0.197713762	-0.17	43.169	-0.184649281	-0.17
44.184	-0.210577254	-0.17	44.184	-0.147120206	-0.17
45.199	-0.211584209	-0.17	45.199	-0.166080062	-0.17
46.213	-0.199698358	-0.17	46.213	-0.168688627	-0.17
47.228	-0.248931213	-0.17	47.228	-0.252037261	-0.17
48.242	-0.162753158	-0.17	48.242	-0.138284041	-0.17
49.257	-0.226487371	-0.17	49.257	-0.147730613	-0.17
50.271	-0.19886561	-0.17	50.271	-0.182657969	-0.17
51.286	-0.191672478	-0.17	51.286	-0.249715167	-0.17
52.301	-0.192145245	-0.17	52.301	-0.181643111	-0.17
53.315	-0.228227478	-0.17	53.315	-0.132198188	-0.17
54.33	-0.135567442	-0.17	54.33	-0.158077101	-0.17
55.344	-0.196743244	-0.17	55.344	-0.20379568	-0.17
724.977	14.68213985	14.637	724.977	16.35891506	16.57
725.992	14.57358998	14.637	725.992	16.51709393	16.57
727.006	14.68397197	14.637	727.006	16.58589748	16.57
728.021	14.63061624	14.637	728.021	16.60245739	16.57
729.035	14.55845899	14.637	729.035	16.54309278	16.57
730.05	14.5785534	14.637	730.05	16.44268414	16.57
731.065	14.63127404	14.637	731.065	16.56721847	16.57
732.079	14.64882637	14.637	732.079	16.70140054	16.57
733.094	14.54051841	14.637	733.094	16.61988398	16.57
734.108	14.65651409	14.637	734.108	16.49448137	16.57
735.123	14.71285461	14.637	735.123	16.56808195	16.57
736.138	15.08866249	14.637	736.138	16.02728215	16.57
724.977	14.68213985	14.637	724.977	15.34916677	16.57
725.992	14.57358998	14.637	725.992	15.17789982	16.57
727.006	14.68397197	14.637	727.006	16.35891506	16.57
728.021	14.63061624	14.637	728.021	16.51709393	16.57
729.035	14.55845899	14.637	729.035	16.58589748	16.57
730.05	14.5785534	14.637	730.05	16.60245739	16.57

731.065	14.63127404	14.637	731.065	16.54309278	16.57
732.079	14.64882637	14.637	732.079	16.44268414	16.57
733.094	14.54051841	14.637	733.094	16.56721847	16.57
734.108	14.65651409	14.637	734.108	16.70140054	16.57
735.123	14.71285461	14.637	735.123	16.6198398	16.57
736.138	15.08866249	14.637	736.138	16.49448137	16.57

The RMSE calculated using the equation above and the temperatures shown in the table above for each bath is 0.053 and 0.074 °C for the first two baths at the 15:10 time slice. The RMSE is 0.14 °C, for the bath at the far end of the cable (Bath 3), approximately twice that of the baths at the beginning of the cable and is a result of few photons being returned from the distant end of the cable, and therefore more noise in the returned signal.

For the 4:28 time slice, the RMSEs for the baths near the start of the cable are similar (0.039 and 0.069 °C) to the previous time and consistent with expectations. However, the RMSE for the far calibration bath during the nighttime trace is 0.40 °C; much higher, and suggests that the cable loop in the stream was not at a uniform temperature. Most of the RMSE is derived from one measurement in the middle of the calibration coil which is ~1 °C colder than all the rest of the measurements. Likely reasons may be that this portion of the cable was not in good contact with the stream or may have been partially exposed above the water surface during the night time due to a change in river stage or other disturbance. These data point out the value of looking closely at all of the data and investigating anomalous readings.

[Return to Exercise 2](#) ↑

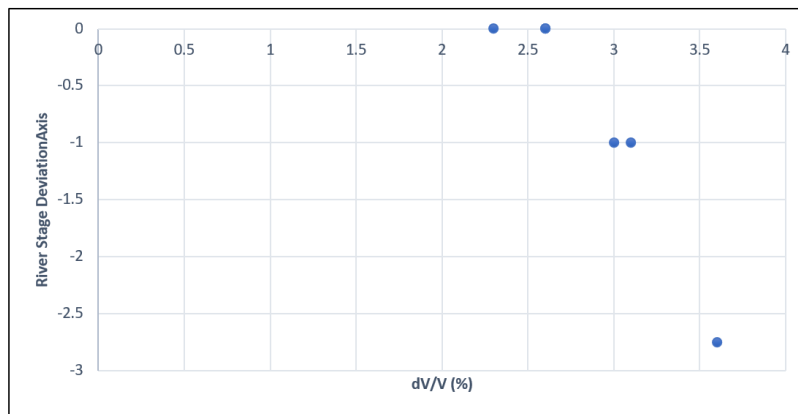
### Solution Exercise 3

In the table below, we have taken (by eye) 6 pairs of stage and % change in seismic velocity from Figure 12. You may chose different times, but try to pick enough times that you span the range of river stage and % change in seismic velocity. The data are presented in the table and plotted in the graph below. Note that we have “estimated” the stage to a precision of 0.1 m and the velocity change to a precision of ~0.25 from the figure. Using these data below, a least squares regression equation can be fit (using Excel or by hand) to the data to relate % velocity change to river stage. Using the points below, the regression equation is approximated below and suggests a fairly robust relation between changes in seismic velocity and the proxy (river stage) for depth to groundwater.

$$dv/V(\%) = -2.2 * \text{stage} + 5.5, R^2 = 0.9$$

Reported river stage and corresponding normalized change in seismic velocity

Date	Stage (m)	dv/V (%)
10/25/17	2.3	0
11/19/17	3.0	-1
12/04/17	2.6	0
01/10/18	3.6	-2.75
01/28/18	3.1	-1
02/22/18	2.6	0



Observed change in normalized seismic velocity related to river stage fluctuations.

[Return to Exercise 3](#) ↑

## 9 Notations

$C_e$	calibrated Brillouin frequency shift strain coefficient of the fiber ( $T^{-1}$ )
$C_p(\theta)$	soil heat capacity ( $ML^2T^{-2}\theta^{-1}$ )
$c_s$ and $c_{as}$	Constants related to laser power and responsiveness of the DTS detectors ( $ML^2T^{-2}$ )
$C_T$	calibrated Brillouin frequency shift temperature coefficient ( $\theta^{-1} T^{-1}$ )
$\Delta\alpha$	difference in attenuation factors between Stokes and anti-Stokes ( $L^{-1}$ )
$\Delta\varepsilon$	change in strain (dimensionless, $LL^{-1}$ )
$\Delta\nu_B$	change in Brillouin frequency ( $T^{-1}$ )
$\Delta T$	change in temperature ( $\theta$ )
$\gamma(\theta)$	soil thermal conductivity ( $MLT^{-3}\theta^{-1}$ )
$\hbar$	reduced Planck's constant ( $ML^2T^{-1}$ )
$I_{as}$	measured photon intensity of anti-Stokes ( $ML^2T^{-2}$ )
$I_s$	measured photon intensity of Stokes ( $ML^2T^{-2}$ )
$k$	Boltzmann constant ( $ML^2T^{-2}\theta^{-1}$ )
$\lambda_s$ and $\lambda_{as}$	wavelengths of the Raman shifted returning light (L) as discussed by Farahani and Gogolla (1999)
$\Omega$	frequency difference between Stokes and anti-Stokes scattering in typical fiber ( $T^{-1}$ )
$\rho$	water density ( $ML^{-3}$ )
$\theta$	soil volumetric water content (dimensionless, $(L^3L^{-3})$ )
$z$	distance along the optical fiber (L)

## 10 About the Authors



**Dr. Scott W. Tyler** is a Foundation Professor in the Department of Geological Sciences and Engineering at the University of Nevada, Reno and co-director (with co-author John Selker) of the National Science Foundation-supported Centers for Transformative Environmental Monitoring Programs (CTEMPs) Community User Facility focusing on the development and application of fiber-optic based sensing for environmental temperature and strain. His research spans the atmospheric boundary layer, through the vadose zone and has included deep groundwater circulation.

With training in mechanical engineering and hydrogeology, his research is focused on water, solutes, and energy fluxes in the subsurface, as well as their exchange into the. Along with colleague and friend, John Selker from Oregon State University, he leads the NSF-supported CTEMPs, making DTS systems and training available to the hydrologic and earth science community. His recent work focuses on the measurement of the dynamics and thermal evolution of Antarctic ice shelves and the ocean waters below. As part of the NSF-supported TARSAN project, he helped developed fiber-optic moorings on the Thwaites Glacier and developed a distributed acoustic monitoring system for both the ice shelf and the underlying ocean which has been operating at Thwaites since 2020.



**Dr. John S. Selker** is a Distinguished Professor of Biological and Ecological Engineering, Oregon State University, focused on Water Resources Engineering. His areas of expertise include vadose zone and groundwater systems, electronic design, and development projects. In addition to his CTEMPs role, he is co-director of the Trans-African Hydro-Meteorological Observatory (TAHMO) with co-Author Nick van de Giesen, which aims to develop a continental-scale network of weather stations across Africa. He has worked in the USA, Kenya, Somalia, Sri Lanka, Canada, Chile, and England and carried out research in Chile, Ghana, Senegal, Israel, China, and 10 European countries. Dr. Selker has published 230 peer-reviewed articles. In 2013, he was elected Fellow of the American Geophysical Union and received the John Hem Award for Science and Technology from the American Groundwater Association, then in 2020 he was elected

President of the American Geophysical Union Hydrology Section, a position previously held by Scott Tyler.



**Nick van de Giesen** received the Kandidaats Bachelor of Science degree and the Master of Science degree in Land and Water Management from Wageningen Agricultural University (currently, named: Wageningen University & Research), Wageningen, The Netherlands, in 1984 and 1987, respectively, and a Ph.D. from Cornell University in 1994. After a postdoctoral position with the West Africa Rice Development Association, Bouaké, Côte d'Ivoire, he was a Senior Researcher for six years with the Center for Development Research (ZEF), University of Bonn, Bonn, Germany, where he was the Scientific Coordinator of the Global Change in the Hydrological Cycle Volta Project. Since 2004, he has been with the Water Resources Section, Faculty of Civil Engineering and Geosciences, Delft University of Technology, where he currently holds the "Van Kuffeler" Chair of Water Resources Engineering. Since January 2015, he has been chairman of the Delft Global Initiative. With Dr. Selker, he is co-director of the [Trans-African Hydro-Meteorological Observatory](#) (TAHMO) and a member of several international scientific advisory boards. He is the scientific head of the Sustainable Development Goals route of the Netherlands National Science Agenda. His research interests concern new environmental observation methods, such as Distributed Temperature Sensing, and computational hydrology ([www.ewatercycle.org](http://www.ewatercycle.org)).



**Dr. Thom Bogaard** is an Associate Professor at the Delft University of Technology, Department of Water Management and at IHE Institute for Water Education, Delft. His research focuses on hydrology and geomorphology. He likes to work on multidisciplinary problems including hydrology, water quality, geomorphology and ecology. He is specialized in soil, hillslope and landslide hydrology as well as in the development and application of innovative measurement techniques for hydrology, such as applying fiber optic cable in hydrogeomorphological studies and developing nanoparticles with DNA-tags that can be used as water flow path tracers. Thom Bogaard works on several capacity-building projects with local universities and knowledge institutes in Southeast

Asia, Africa and South America. He serves as executive editor of the open-access Hydrology Earth System Sciences journal and associate editor of Wires Water.



**Dr. Juan Pablo Aguilar-López** is an Assistant Professor in the Hydraulic Engineering Department of the Delft University of Technology. He is interested in the use and implementation of technology (open hardware, innovative sensors and machine learning) in structure design and operation for flood risk management. He has an M.Sc. in hydroinformatics and a Ph.D. in probabilistic design of multifunctional flood defenses. Since the start of his career, Dr. Aguilar-López has been interested in the use of real-time monitoring of flood management structures and the post-processing of these measurements via surrogate modeling for structural operation. He aims to improve and develop methods to monitor and quantify flood risk and resilience and to incorporate resilience in designs for flood risk reduction in cities and urban regions, including both grey and green (nature-based) interventions. The combination of real-time monitoring and data-driven modeling allows a fast and accurate diagnosis of a flood defense system for operation. This is of paramount importance for flood risk managers and stakeholders as it makes flood defense systems more flexible and resilient, and can be used for risk reduction, early warning, evacuation decisions and even asset management.

Please consider signing up for the GW-Project mailing list to stay informed about new book releases, events and ways to participate in the GW-Project. When you sign up for our email list it helps us build a global groundwater community. [Sign up](#).



# Modifications to Original Release

## Changes from the Original Version to Version 2

Original Version: July 2022, Version 2: March 2023

### **General changes:**

Added Modifications section

Updated Table of Contents after revision

### **Specific changes:**

page numbers refer to page numbers in the original pdf

page i, corrected page numbering of front matter so there were not two pages numbered with i

page ii, updated copyright format and enhanced copyright information

page 3, Figure 1 caption, italicized variables  $T$ ,  $\lambda$ , and  $\varepsilon$

page 7, 2nd paragraph, line 5, italicized subscripts  $s$  and  $aS$

page 8, sentence before Equation 1, italicized variable  $T$

page 8, Equation 1 and variable definitions,  $h$  corrected to  $\hbar$

page 8, Equation 2, italicized variable  $C$  in the denominator

page 9, Figure 3 caption, added recognition that figure is from Encyclopedia Britannica

page 14, Equation 3, italicized variable  $D$  and removed space after  $D$

page 14, Equation 3 and variable definition, subscripted  $p$  of  $Cp$

page 14, 1st line of last paragraph, changed uppercase theta ( $\theta$ ) to lowercase ( $\theta$ )

page 15, Figure 7 caption, italicized  $T_{cum}$  to  $T_{cum}$

page 20, line before Equation 4, corrected the year of Zhang and others to 2020

page 20, Equation 4, and its variable definitions, changed variables  $vB$ ,  $C_e$ ,  $CT$  to  $v_B$ ,  $C_e$ ,  $C_T$

A

page 20, definition of  $\Delta vB$ , corrected "échange" to "change"

page 27, list item d), replaced all occurrences of sec with s

page 28, after the figure of Exercise 2, revised the sentence "The data provided in the spreadsheet ↗ can be used to undertake the following tasks." to "The data for this exercise are provided in a spreadsheet that can be downloaded by visiting the web page for this book at [gw-project.org/books/distributed-fiber-optic-hydrogeophysics/](http://gw-project.org/books/distributed-fiber-optic-hydrogeophysics/) ↗ and clicking the "Download" button."

page 28, list item a), italicized variables  $\gamma$ ,  $\alpha$ , and  $C$  in first and last sentence

page 28/29, list item a) 1<sup>st</sup> sentence, after "the method of Hausner and others (2011)", added "as described by Equation 2"

page 29, Exercise 3, italicized  $dv$  and  $V$

page 30 through 37, left justified references

page 37, deleted the first of the two references to Zhang and others (2020), keeping the one with the proper format

page 38, list item c), italicized the subscripts of  $T_i$ ,  $T_o$  and  $Q_i$

page 38, last equation, replaced three occurrences of sec with s

page 39, list item d, 6th line, italicized subscripts of  $T_o$  and  $T_i$

page 39, 3rd equation, inserted °C after 0.10 in numerator

page 39, 4th equation, un-italicized both occurrences of  $C$  in the denominator

page 39, last paragraph, italicized subscripts of  $Q_i$  and  $Q_g$

page 41, definition for  $T(z_i)$ , deleted "represents the"

page 41, definition of  $T_{bath}$ , remove the o in front of  $T_{bath}$ , and deleted "represents the" from the definition

page 45, Notations:

subscripted e of  $C_e$

changed uppercase  $\theta$  to lowercase  $\theta$  in the variables  $C_p(\theta)$  and  $\gamma(\theta)$

subscripted T of  $CT$

subscripted B of  $\Delta vB$

removed italic font from  $\hbar$

page 45, definition of soil thermal conductivity, removed the first power on L in the dimensions

Supplementary files Exercise2-DTS-data-calibration.xlsx and Solution-Exercise2-DTS-data-calibration.xlsx, worksheet DTS RAW, changed delat to delta in cells E25 and K25

### Changes from the Version 2 to Version 3

Version 2: 23 March 2023, Version 3: 25 March 2023

#### Specific changes:

page numbers refer to page numbers in the version 2 pdf

page 8, added “reduced” before Planck’s constant

### Changes from the Version 3 to Version 4

Version 3: 25 March 2023, Version 4: 26 March 2023

#### Specific changes:

page numbers refer to page numbers in the version 3 pdf

page 45, changed  $h$  to  $\hbar$  and added “reduced” before Planck’s constant